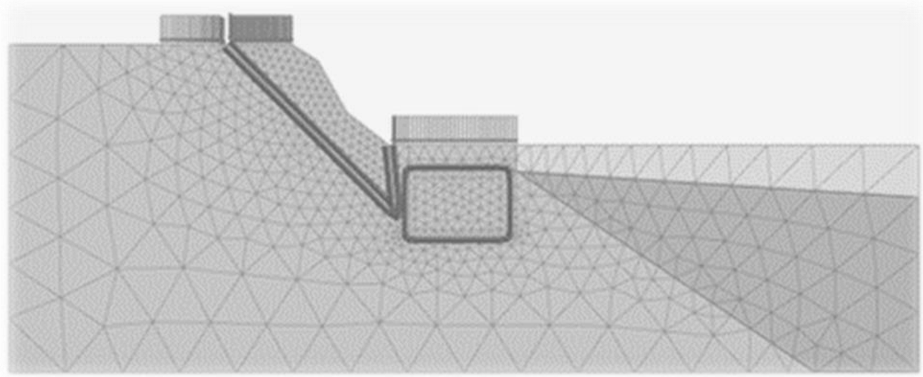

Analysis of force and strain distribution in soil and concrete tunnel due to a planar rock movement

Master's Thesis in the Master's Programme Infrastructure and Environmental Engineering

SION MATHEW
MOSTAFA GHAFFARIAN MAHDOODI

DEPARTMENT OF ARCHITECTURE AND CIVIL ENGINEERING

CHALMERS UNIVERSITY OF TECHNOLOGY

Gothenburg, Sweden 2022
www.chalmers.se

MASTER’S THESIS ACEX30

Analysis of force and strain distribution in soil and concrete tunnel due to a planar rock movement

Master’s Thesis in the Master’s Programme Infrastructure and Environmental Engineering

SION MATHEW
MOSTAFA GHAFFARIAN MAHDOODI

Department of Architecture and Civil Engineering
Division of Geology and Geotechnics
CHALMERS UNIVERSITY OF TECHNOLOGY
Göteborg, Sweden 2022

Analysis of force and strain distribution in soil and concrete tunnel due to a planar rock movement

Master’s Thesis in the Master’s Programme Infrastructure and Environmental Engineering

SION MATHEW
MOSTAFA GHAFFARIAN MAHDOODI

Examensarbete ACEX30
Institutionen för arkitektur och samhällsbyggnadsteknik
Chalmers tekniska högskola, 2022

Department of Architecture and Civil Engineering
Division of Geology and Geotechnics
Chalmers University of Technology
SE-412 96 Göteborg
Sweden
Telephone: + 46 (0)31-772 1000

Department of Architecture and Civil Engineering
Göteborg, Sweden, 2022

Analysis of force and strain distribution in soil and concrete tunnel due to a planar rock movement

Master's thesis in the Master's Programme Infrastructure and Environmental Engineering

SION MATHEW
MOSTAFA GHAFFARIAN MAHDOODI

Department of Architecture and Civil Engineering
Division of Geology and Geotechnics
Chalmers University of Technology

ABSTRACT

Rock movement in the vicinity of existing structures and infrastructure projects is of great importance as it can lead to major damages and loss if care is not taken. The response in the tunnel due to such movement has to be monitored and actions taken to prevent major loss. The aim of the study is to examine how a thin soil column and a concrete tunnel will be affected by a planar rock movement and thereby determine the location for placing a deflection measurement system in the right wall of the tunnel. The goal of the report is to act as an example for future studies regarding rock movement and its impacts on thin soil sections as conventional theories cannot be applied in such cases. To exemplify this, the case of an existing rock slope in Kvarnberget, Gothenburg where a cut-and-cover tunnel is planned to be constructed has been taken into account. The analysis was conducted both analytically and numerically.

A planar fault in the rock was assumed along which failure would happen in order to simplify the analysis conducted analytically and as the numerical analysis was performed in 2 dimensions. In the analytical method, the forces acting on the rock block was determined, and the weight of the rock block was calculated. A theory was adopted to determine the failure in the thin soil column. Subsequently, the forces acting on it determined and the conditions of equilibrium of forces applied in the failure section. Following this, the lateral forces acting on the tunnel were determined, and a structural analysis performed to calculate the deflection taking place in the tunnel due to the rock movement. The numerical analysis performed using the software PLAXIS where some material properties were obtained from laboratory results while others were assumed. Several scenarios were created to understand how the results would vary accordingly.

From the numerical analysis, it was found that the failure wedge assumed in the soil column while performing the analytical analysis was similar. On comparing both analyses it was found that the results from the analytical results showed higher deflection. The point of maximum differential stress at the right wall was calculated to be at the intersection between the top and right wall and it was concluded that the deflection measurement had to be placed there.

Key words. **Rock movement, cut-and-cover tunnel, deflection measurement system, soil wedge, numerical analysis**

Contents

Preface

The following report is authored by two students from the master's programme Infrastructure and Environmental Engineering at Chalmers University of Technology during the spring semester 2022. The study was conducted within the division of Geology and Geotechnics with supervision of Ayman Abed, Senior lecturer at the department of Geotechnics. The project has been carried out in collaboration with Norconsult AB.

We would like to extend our sincere gratitude to our supervisor Ayman Abed, who is an expert in numerical analysis for giving us the confidence, support, and guidance throughout the project. Further, we would like to acknowledge our examiner Minna Karstunen for raising our interest in numerical modelling. Additionally, we want to express our gratitude to Norconsult AB for defining a suitable thesis for us and to Per Eriksson and Sara Bergqvist for their involvement and support for our study.

Chalmers University of Technology
Göteborg June 2022

Sion Mathew
Mostafa Ghaffarian Mahdoodi

Notations

Roman upper-case letters

E	Young's Modulus
EI	Bending stiffness
E_{oed}	Oedometer modulus
E_r	The final resultant force by rock movement
E_t	The lateral resultant force on the tunnel
F1	Frictional resistance force at the top of the tunnel
F2	Frictional resistance force at the bottom of the tunnel
G	Shear modulus
K	Bulk modulus
K_0	Coefficient of earth-at-rest pressure
L	Length of the member
M	Moment
M'	Carryover moment
N	Normal force
R	The reaction force on the slip plane
R-inter	Strength reduction factor for soil-structure interaction
S	Sway force
S'	Arbitrary sway force
S_s	Soil strength
S_c	Strength of the contact surface between soil and stiff material
T	Shear force
T_{r-max}	Maximum resistance force
U	The lateral water pressure on the tunnel
U_r	Water pressure resultant force
W	Weight of the soil wedge plus the traffic load on the surface
W_r	Weight of the rock block per running meter

W_T	Weight of the rock block plus the building load

Roman lower-case letters

c	Cohesion of discontinuity infilling
c_f	Cohesion of the filling material
h	Vertical distance
h_w	Height of the water level
k	Stiffness of the member
k_s	Sway correction factor
l_b	Inner height of the rock block perpendicular to the discontinuity
l_v	Length of the discontinuity
l_{v-w}	Length of discontinuity which is filled by water
q_b	Load of the building per running meter
q_0	Uniform distributed load on top of the tunnel
q_1	Minimum distributed load on the left wall
q_2	Maximum distributed load on the left wall
q_3	Minimum distributed load on the right wall
q_4	Maximum distributed load on the right wall
q_5	Minimum distributed load on the bottom of the tunnel
q_6	Maximum distributed load on the bottom of the tunnel
u_0	Water pressure
z	Height of the soil

Greek letters

α	The angle of slip plane (CD) with the horizontal
β	Angle of the wall
θ	Angle of the discontinuity
θ_A	Slope of point A
σ	Normal stress

σ_{max}	Maximum principal stress
γ	Unit weight
γ_w	Unit weight of water
γ_r	Unit weight of the rock
φ	Friction angle
φ_f	Friction angle of the filling material
δ	Angle of the lateral resultant force on the tunnel (E_t) with the horizontal
ε	Angle of slope on top of the soil
υ	Poisson's ratio
μ	Friction coefficient
τ	Shear stress
ψ	Dilatancy angle
Δ_{q1}	Displacement by q1
Δ_{q2-q1}	Displacement by (q2-q1)
Δ_{q3}	Displacement by q3
Δ_{q4-q3}	Displacement by (q4-q3)
Δ_B	Displacement at point B (Independently)
Δ_C	Displacement at point C (Independently)
Δ	Total displacement of the frame

Abbreviations

FE	Finite element
FEM	Finite element method

List of figures

List of Tables

1

Introduction

1.1 Background

Rock masses usually consist of faults, discontinuities, joints, and other mechanical defects which are formed by a wide range of geological processes throughout their history (Priest, S. D. ,1993). Designing any structure in rock mass requires considering discontinuities when the stability of structure is assessed. The days when long years of experience, and analytical solutions of simple continuum models alone could design structures in such situations are gone with the emergence of modern numerical tools like the finite element method (FEM). Finite element modeling software are of great interest as it can model the mechanisms of soil–structure interaction as well as accommodate realistic soil and rock behavior. Thanks to the FEM, modelling complex sections, geometries, and conditions have become much easier, faster and moreover, much more accurate.

The Göta Älv river valley in Gothenburg is characterized by some geological and topographic conditions including layers of clay that superpose cohesionless soil and bedrock (SGI, 2012). An 8-kilometer-long double-track underground railway tunnel is being constructed in this location (Trafikverket, 2022). Of the 6-kilometer underground section, 4 km will run through rock and 2 km through the clay (Trafikverket, 2021). The tunnel will be built using the cut-and-cover technique in the shallow sections and a rock tunnel will be built using the drill-and-blast technique in deeper sections. The section at Kvarnberget is shallow and a cut-and-cover tunnel will be constructed after rock cutting and excavation.

In this study, the effects of the rock movement due to planar sliding in the vicinity of this concrete tunnel at Kvarnberget are investigated using two models; a numerical model using the FEM software PLAXIS in two dimensions, and an analytical model. Different cases for the problem are determined to investigate probable situations and understand the effects of rock movements on the tunnel.

1.2 Aim

This thesis is intended to evaluate the force and strain distribution in soil and on a concrete tunnel due to a planar rock movement using the finite element modelling software PLAXIS in two-dimensions. Consequently, the suitable positioning of a deflection measurement device on the right wall of the tunnel could be identified by calculating maximum differential stresses. The conditions for modelling were assumed to be similar to that of the ongoing railway tunnel project in Gothenburg. In order to compare the results obtained from the numerical model, an analytical model considering the rock movement has to be developed. If the investigation could accurately determine the effects on the concrete tunnel stress field caused by even small rock movement pressing against the tunnel, measures could be taken at the proper time and location to avoid expensive damages. Keeping this in mind, the following research questions have been formulated:

- To what extent does the rock movement have an impact on the concrete tunnel?

- At what position is the deflection measurement device to be placed on the right wall?
- How do the results obtained from the analytical and finite element models correspond to each other?

1.3 Methodology

This study has been conducted by creating a finite element simulation by studying and selecting the appropriate models for soil layers and rock. The idea is to generate a close-to-life scenario in PLAXIS 2D Version 21 in two dimensions using geologic and hydrologic data collected site conditions and from similar studies conducted previously. The data which was used to set up the model includes:

• The stratigraphy of the area and properties of constituent layers

• Groundwater levels

• Details of excavation

• Properties of the tunnel and material properties

The geometry of the numerical model is created by defining the soil stratigraphy and a planar discontinuity in the rock. Loads from the road, which are planned above the tunnel, and from the adjacent building is applied in the model. The investigation is also conducted by considering the results from the mesh and parameter sensitivity analyses of the model using several scenarios with different conditions. To compare the results and verify the numerical model, an analytical model has been developed as well. For this purpose, firstly all involved forces are identified. An extension of Coulomb’s theory is adopted to investigate the soil failure caused by the rock movement pressure and to understand how the force from rock movement would be conveyed through the soil gap and affect the tunnel. In Figure 1.1, a flowchart of the whole process is illustrated.

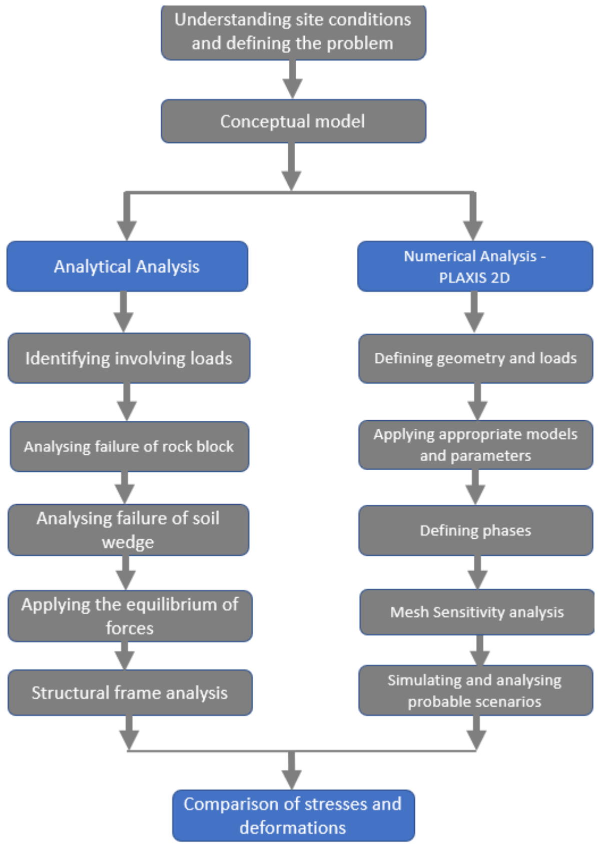

Figure 1.1. Methodology flowchart

1.4 Limitations

Generally, 2D modelling follows many assumptions and hence has its limitations. Indeed, modelling discontinuity in rock properly requires a 3D model which considers all the fractures that might exist in all directions, hence, one of the significant limitations of this study would be 2D modelling in PLAXIS. Moreover, due to the lack of data, some of the material parameters had to be assumed and adopted from reliable literature which distances the model from being an exact simulation of the site conditions at Kvarnberget. Regarding modeling the discontinuity in rock, although the latest version of PLAXIS includes the discontinuity feature for this purpose, it had been modeled using the interface feature as the updated version was not available.

2

Input for modelling

A good understanding of the area surrounding the construction at various stages of excavation and the soil structure interaction is important for proper analysis. Hence, it is vital to gather all available information of previous borings, rock faults and other desk studies conducted in the area. An area surrounding Kvarnberget was chosen as the study site since the tunnel construction was planned to be constructed close to the rock face and had numerous fracture planes in it. A consistent textural foliation is observed in the bedrock all over Gothenburg with its strike roughly parallel to the Göta Älv river at Kvarnberget. The rock at the site is composed of a high-grade metamorphic rock called gneiss. Excavation in rock would be done below this surface to a depth of 15 metres for the construction of the tunnel and then casting of the tunnel would be done in concrete in the open shaft. The newly excavated rock face at the section of interest showed 3 major failure planes and the presence of a major failure wedge that could move towards the tunnel. The Navigation school and another residential building which have their foundations on rock lie in close proximity to the rock face and it is assumed that the buildings would contribute to a load of 70 kN/m^2. The tunnel would have outer dimensions of 15 x 10 metres and have a thickness of 1 metre. Once the construction was done, the tunnel is planned to be backfilled with friction soil over the roof of the tunnel, 4 metres in depth. This would create a gap of 1.5 metres filled with soil between the tunnel and rock. A road is planned over the tunnel and the traffic load expected on the roof slab from the road is 22 kN/m^2. The right side of this section consists of rock at a lower height overlaid by clay and soil. It was assumed that in the permanent stage, the groundwater level in the rock section was at +5.5m with respect to the mean sea level whereas it was reduced to +1m in the reaming section.

3

Literature review

3.1 Failure mechanisms

Studies have been conducted regarding analytical methods for evaluating the active thrust exerted by a narrow backfill behind a retaining wall which is built near a rock face. (Greco V, 2013) examined three different failure mechanisms for this kind of situation. In the first mechanism based on the failure Coulomb theory, due to the wall movement, the failure planes inside the narrow backfill behind the wall will be along two surfaces starting from the wall heel, one at the contact with the retaining wall and the other inside the backfill soil at an unknown angle. In the second mechanism, it is assumed that the rock face is closer to the wall, then the failure plane intercepts the rock face, and the failure wedge will be formed by two blocks. In the case which the rock face is even closer to the wall, the failure plane intercepts the wall back face, and the failure wedge will be formed by three blocks as the third mechanism. Then the limit equilibrium method is used to determine the lateral earth pressure in each case and results are compared with some experimental and numerical models (Greco V, 2013). In Figure 3.1, these three failure mechanisms are shown.

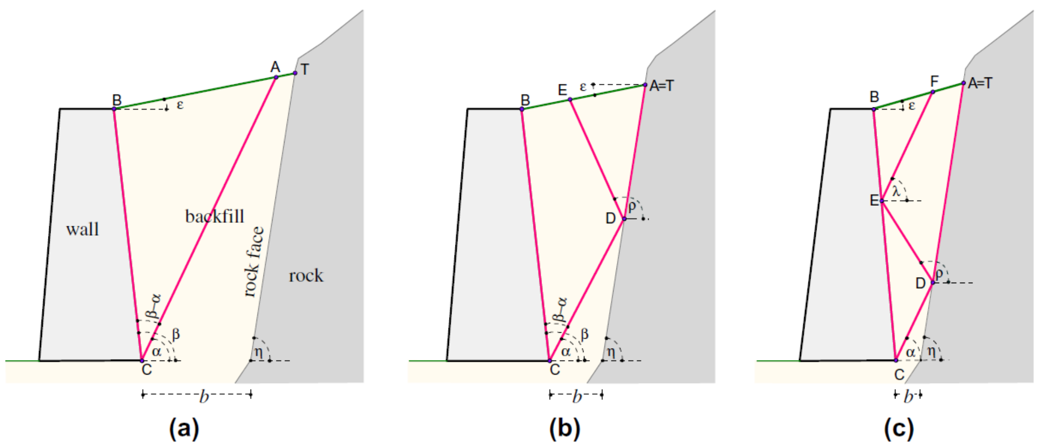

Figure 3.1. Thrust wedges and slip planes (in red) for Mechanism 1 (a), Mechanism 2 (b), and Mechanism 3 (c). (Greco V, 2013).

(Chen et al, 2018) also conducted a similar study for a narrow backfill between a retaining wall and a rock face. They generated a finite element model which showed that shear bands occur inside the soil when it fails. They investigated the effect of ratio width/height on the failure mechanism and intensity of shear dissipation happening inside the backfill. According to the finite element results, the failure mechanism of the narrow backfill shown in Figure 3.2 can be closely related to the width/ height of backfill and friction angle at the soil-wall interface. In the failure state, as it can be seen in Figure 3.2, the backfill soil can be divided into two parts. The first part is the upper zone, in which shearing happens along the soil-wall interface, and the second part is lower zone with shearing inside the backfill.

They also made analytical calculations using the equilibrium of forces to calculate the lateral pressure in different cases. To obtain the inclined angle between the shear bands and the horizontal, the calculation process is simplified by using the Coulomb equation since it is proved that error of this equation is less than

15%. The other impressive part of their study was the investigation of the effect of internal friction angle of the soil and the soil-wall interface friction angle on the number of reflective shear bands in the backfill. (Chen et al ,2018)

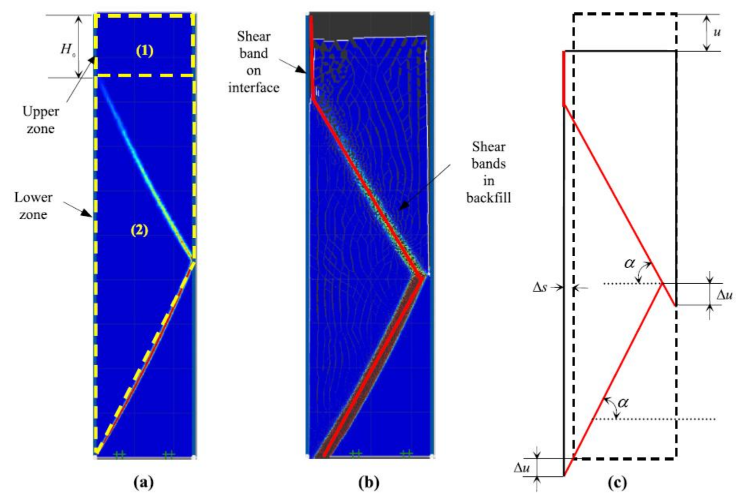

Figure 3.2. Failure state of narrow backfill (Chen et al ,2018)

Rahardjo P. P. facilitated the use of the finite element modelling software PLAXIS 2D to simulate the weathering of breccia on claystone. The aim of Rahardjo`s simulation was to calculate the movement caused by the sliding of the claystone layer on the breccia layer. In order to simulate the landslide, an interface element was used in the boundary between breccia and the claystone. Initially, the breccia layer was assumed to be stable, followed by placing fill material on top of the sliding area. The value of the interface strength R-inter was changed until movement started in the breccia layer. The movement predicted by the model was lower than the measured data and this was because the computer simulation doesn't continue after failure (Rahardjo P, n.d.).

Gong L. et.al modelled two-dimensional direct shear tests of laboratory scale infilled rock joints using the finite element modelling software FLAC 2D. Models with three levels of joint roughness were simulated with speswhite kaolin as the infilling material. The simulation of the planar joint in the paper was of interest as it was similar to the problem in this study. The system was simulated as a block with infilling sandwiched in-between them. The discontinuity was designed using AutoCAD and the sides of the upper block as well as the left side of the lower block were fixed in the x-direction, whereas the bottom boundary fixed in the y-direction (Gong, Ren , & Nemcik, 2018).

3.2 General

3.2.1 Soil and rock

The state of clay can vary from a slurry to a hard-sounding stone (clay shale) with the decrease in water content. Similarly, the transition from soil to rock can be seen to be as fluid, involving rock -like soils and rock (Gerlymatou E., 2020). In that sense, the boundary between soil and rock is unclear. When soil can be seen as a continuum, the discontinuities present in rock make it discontinuous. Soils often appear to represent ductility while rocks respond to loading in a brittle manner except under extremely slow deformation, high pressures, and high temperatures. For very small deformations, some rocks can be considered as elastic, and their elastic domain is somewhat larger than that of soil. Rocks also exhibit extensive anisotropic behaviour due to their geological history. This anisotropy influences the mechanical characteristics of the rock due to the significant reduction of shear strength parallel to the surfaces and the tensile strength normal to them. Rocks move parallel to the intersections of the interface groups leading to higher resistance to internal rotation. Hence, rock mass has lower degree of freedom in terms of movement compared to soils (Gerolymatou E., 2020). The test values obtained from a core boring giving an undisturbed sample of soil can be considered to represent the engineering properties of the soil, whereas in rock, a clear division must be made between the engineering properties of intact rock and that of the rock mass where the discontinuities are considered (Parker H, 1996).

Rocks are mainly classified according to their origin as sedimentary, igneous and metamorphic rock. Igneous rock is formed by the melting of rock in the deep crust and upper mantle followed by crystallization of the magma or lava. Sedimentary rocks are formed due to the weathering and erosion of rocks at the surface followed by deposition, burial and lithification. When rocks are subjected to extreme temperatures and pressures in the deep crust and the upper mantle and subsequently recrystallize into a solid state of new minerals, metamorphic rocks are formed. Gneiss, which is the type of rock observed at the study site is a metamorphic rock having a coarse crystalline texture and a foliated structure.

3.2.2 Rock

Rock mass as a whole is a combination of intact rock, fractures, foliations and defects. Foliations are repetitive layering usually seen in metamorphic rocks due to the history of loading and deformation, while discontinuities are surfaces that disrupts the rock mass continuity. The spatial arrangement of discontinuities in the rock mass divides it into individual rock blocks (Gerolymatou E., 2020).

The anisotropy in the form of discontinuities observed in rock range from a texture or fabric in rock, like foliations to major faults in rock mass. A spatial and geometric configuration of rock constituents, its appearance associated with folding during its formation and its structural and textural occurrence is called rock fabric or foliation. Bedding, banding, heterogeneous fabric, dense interlocking, void spaces anhydrite layers or veins, and microscopic structures such as grain boundaries are examples of fabric. Microscopic fabric structures influence mucking and the cutting ability of the excavator. These fabric structures mobilize local stability of the tunnel excavation by swelling when the threshold stress of micro-crack initiation is exceeded. Veins can prevent the disintegration of surrounding rock mass by arresting the growth of fractures. The separation of rock fragments along their crystal lattices into flakes or small particles by hydration/swelling is called slaking and it presents a great challenge while tunneling. The rock type, temperature of the environment and humidity conditions can influence slaking, and disintegration or swelling of rock (Ongodia, J. E.,2017).

Physico-mechanical rock strength is reduced when the weak planes of metamorphic rocks are filled with flaky elastic and anisotropic minerals such as mica, chlorite, amphiboles and pyroxenes. Sheet minerals such as serpentine, talc and graphite slide along cleavage and reduces the rock strength. Moisture along with the presence of montmorillonite clay minerals causes swelling/squeezing of the mineral structure and associated construction difficulty such as mudflows leads to face collapses. Joint roughness weakening, core softening and reduction of both strength and wedge interlocking occurs with the presence of clay and their magnitude varies for different clays. Material properties are significant for metamorphic rocks where discontinuities are many because of their formation history (Ongodia, J. E.,2017).

The joints and the interaction between various joint sets affect the kinematic behavior of rock masses. The movement of rock blocks takes place along joints, and thus the movement can only be along the plane defining that joint. The joints change the engineering properties of the rock to a great extent as they determine the kinematic freedom the rock wedges have and affect the rock mass modulus. So, a clear distinction must be made between the engineering properties of the "intact rock" and the engineering properties of the "rock mass", which include the effects of the discontinuities. An intact rock sample from a core boring might not have the discontinuities and their properties are only an upper bound of the behavior of the whole rock mass. So, the relationship between the size of any tested zone and the scale of the discontinuities must be understood and test results must be used appropriately.

Rock characterization must take into account the inherent anisotropy of rock. It must also consider the strong directionality of any engineering properties both in the small scale such as foliation makes the rock anisotropic and also in the larger scale, where the joints and faults make the rock mass behave anisotropic. The origin, nature and propagation of faults determines the level of flexibility and positioning of tunneling project components. Discontinuities intersect to create triangular or irregular separations with isolated rock wedges or rock blocks, respectively and the separations along the discontinuity lines usually coincide with localized shear zones and bedding planes. Faults, fractures, shear zones, bedding planes, folding/bedding planes, joint infilling, foliation, void spaces, degree of saturation, tension cracks and broken/jointed rock directly influence deformation of the rock mass, joints and weak zones. The major discontinuities present in metamorphic rock, identified by mapping and unique trends are salty cleavages which are closely spaced parallel and persistent integral discontinuities in fine-grained strong rock. When the rock is intact, such discontinuities have high cohesion but in fine-grained strong rock, they have persistent planar integral discontinuities (Ongodia, J. E.,2017).

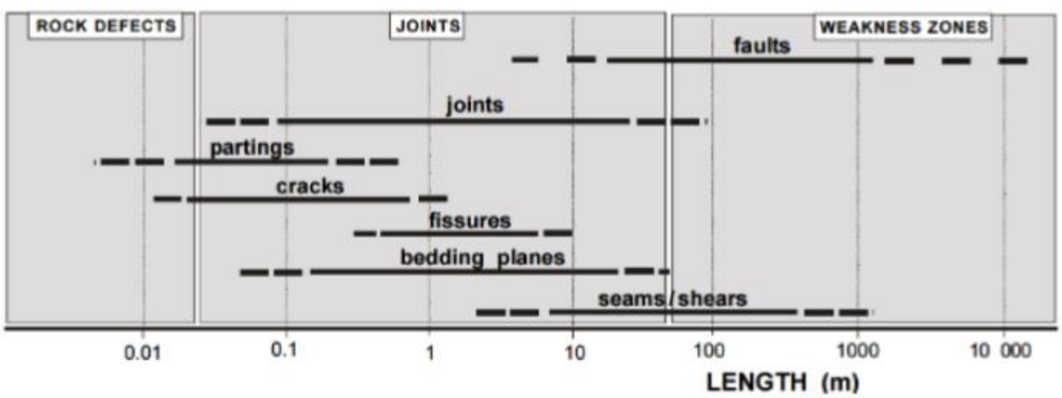

Figure 3.3 Main discontinuities influencing rock mass properties (Ongodia, J. E.,2017).

Rock blocks interact and interlock within each other and place certain constraints on the movement of rock mass due to external forces. Interlocking behavior of the rock blocks can be interrupted by shear zones or persistent discontinuities. In situ stresses is another factor that affects the behavior of the jointed rock system. Stress relaxation during valley erosions can lead to low stresses and can cause open joints to carry water affecting the permeability of the rock mass. Sometimes the shear zone may be impermeable and hold back abundant water on the other side at high heads that will be encountered suddenly during excavation. Thus, the effective permeability of the rock mass is governed by the discontinuities or other defects in the rock rather than the permeability of the intact rock.

Indirect estimation of fracture zone parameters can be done by means of boreholes, of the properties of the components of the zones, i.e. intact rock, fractures and various low-strength materials like fault gouge. Direct observations on the other hand, are done by specifically designed experiments for estimating the properties of fracture zones based on borehole-scale sampling and testing. This is because conventional core drilling technology is not efficient in sampling of poor-quality material commonly encountered in fracture zones and scaling procedures commonly applied to estimate the mechanical properties of individual fractures based on borehole-scale data cannot be directly applied to evaluate the characteristics of fracture zones. Field observations show that fracture zones are characterized by variations in thickness, surface undulations and jogs prevailing on all scales. This infers that the strength- and deformational properties over the plane of the discontinuity can vary locally. No correlation could be established between fracture zones and frictional strength (Leijon B.,1993).

3.2.2.1 Deformation in rock

Bodies under load tend to deform depending on their material properties such as stiffness and strength and it is expressed by the continuum concept called strain. Strain is defined as the change in the body's length, divided by its initial length, provided that the change in the length is small and in one dimension. In two dimensions, strain has three components: the change of length with respect to the length, the change of the height with respect to the height and the average of the change of the length with respect to the height plus the change of the height with respect to the length (Gerolymatou E., 2020).

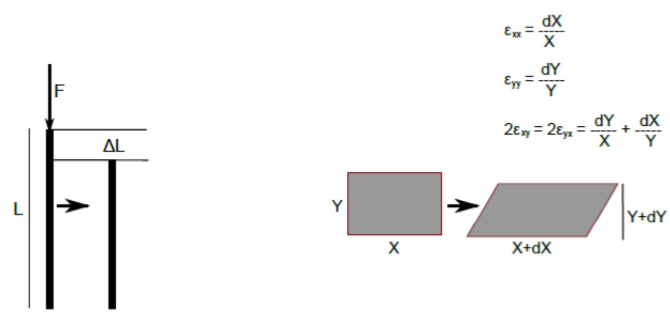

Figure 3.4 One- and two-dimensional strain (Gerolymatou E., 2020)

The force applied per unit surface area is called stress. In one dimension, the orientation of the surface is not considered and only stresses normal to its surface are considered. In two dimensions, both normal and shear stresses are present as the force does not need to act normal to the surface leading to generation of forces along the surface.

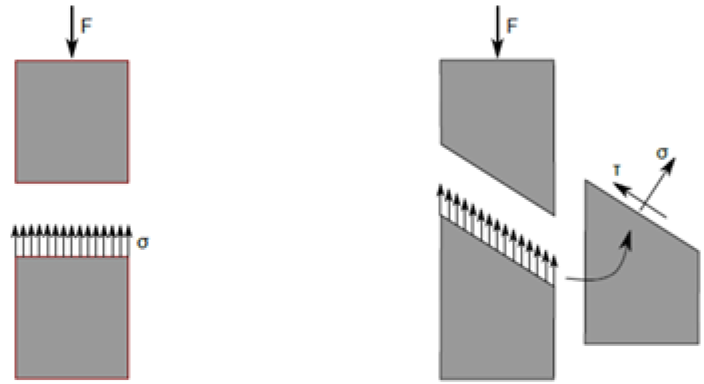

Figure 3.5 One- and two-dimensional strain (Gerolymatou E., 2020)

The initial stress state in the rock before being disturbed is known as the primary stress state. During excavation, the primary stress state is disturbed because of the deflection and changes of the loads and is replaced by a new stress state called as the secondary stress state. The stress redistributions in rock can at times lead to failure of the rock mass. Once the required excavation is done, the rock surfaces are supported or reinforced leading to development of a new stress state called the tertiary stress state.

In a condition when no other forces are acting on the rock other than its weight, the primary stresses can be calculated by its mechanical properties. When the rock mass is transversally isotropic with respect to the vertical axis, its stress state can also be assumed as transversely isotropic. The horizontal stress in such a case is smaller than the vertical stress. The vertical stress can be calculated as a product of the specific weigh of the rock mass and the overburden. On the other hand, the horizontal principal stress can be calculated as the product of the vertical principal stress and a coefficient called the lateral stress coefficient which is less than or equal to 1. It must be noted that the principal stress directions are assumed as vertical and horizontal in this case.

In reality, the in-situ stress state is rarely transversally isotropic, and it cannot be calculated using the lateral stress coefficient. When considering small depths where the ground surface is not horizontal, the principal stress directions are not horizontal and vertical. Geological and tectonic factors can affect the stress state and horizontal stresses may become larger than the vertical stress. The actual vertical stresses can vary from the value calculated using the specific weight of the material. In addition, the lateral stress coefficient is not constant with depth and may be significantly larger than unity.

In the region of a rock slope, the principal stresses are normal and parallel to the slope surface. For an infinitely extended rock slope, the principal stress σ_{max} that is parallel to the surface can be assumed to be the largest and can be calculated as:

$$\sigma_{max} = \gamma h \qquad\qquad eq. 1$$

where γ is the unit weight of the rock and h is the vertical distance to the slope surface (Gerolymatou E., 2020).

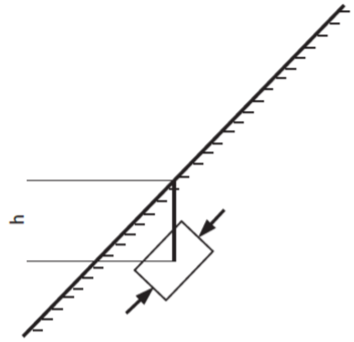

Figure 3.6 In situ stresses under a rock slope (Gerolymatou E., 2020)

3.2.2.2 Strength of discontinuities

The bearing strength in rock is only as strong as its weakest links, which are the joints and fractures. Their strength depends on the relative orientation between the fracture and the stress. Since the strength parallel to the discontinuities is significantly smaller it leads to weaker, more deformable and more strongly anisotropic rock mass. The tensile strength becomes smaller, while the compressibility becomes significantly larger along the direction normal to the discontinuities. Tests have also shown that large number of microscopic cracks join with each another for a crack to propagate (Gerolymatou E., 2020).

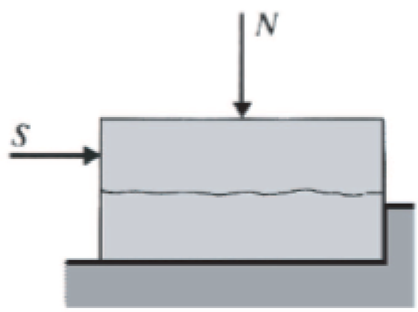

Figure 3.7 Shearing of bodies (Gerolymatou E., 2020).

When two bodies are in touch with each other over a macroscopically smooth surface, as shown in figure 3.7, they are pressed together by a normal force N over the contact surface A. The shear force, acting parallel to the contact surface has to reach a critical value equal to T, for sliding to occur. The shear force and vertical force are related as:

$$T = \mu N \qquad eq. 2$$

Their relation is linear, where μ is the friction coefficient. In 1699, Amontons observed, that μ does not depend on the quality and the roughness of the contact surface and the materials that are in contact.

When calculated in terms per area, the vertical force becomes the normal stress σ and the shear force becomes the shear stress τ. Then the relation is given as:

$$\tau = \mu\sigma \qquad eq. 3$$

Similar test conducted on smooth, clean fracture surfaces showed that the shear stress and vertical stress are related as:

$$\tau = tan(\Phi)\sigma \qquad eq.4$$

where Φ is the effective friction angle of the discontinuities. In reality, discontinuities are not smooth and after a small shear displacement, the maximum value of the shear stress is reached. Beyond that, the shear stress falls with displacement, until it reaches the residual strength. Patton showed that shear and normal forces acting on a such a smooth, clean discontinuity can be related as:

$$S/N = tan(\Phi) \qquad eq.5$$

Filling in fractures of rock influences its shear strength. This can be accompanied by low cohesion and low friction angles of the infilling material. When the discontinuity is filled with materials like clay, silt or sand with thickness larger than the height of the asperities formed by them, the shear strength can be calculated by the properties of the filling material as:

$$\tau = tan\,(\varphi_f\,)\,\sigma_n + c_f \qquad eq.6$$

where φ_f and c_f are the frictional angle and cohesion of the filling material.

When the thickness of the filling material in the discontinuity is smaller than the height of the asperities formed by them, the shear displacement will lead to contact between that sides of the fracture. In such a case, the shear parameters lie between those of the filling and those of the discontinuity (Gerolymatou E., 2020).

3.2.3 Discontinuity infilling

Slope failure in rocks depends on factors like gradient and height of the slope, the geotechnical properties of the material involved, cohesion, degree of weathering and the presence of induced discontinuities and inherent weakness planes. Rainfalls mainly trigger landslides, but over a long time, geological structure, rock weathering and the formation of clay minerals are major reasons. The filling material in rock joints may be detrital material or a geologic filling material that consists of an abraded, soft, pulverized mixture of rock and mineral materials called gouge. This maybe partially to completely loose cohesive or non-cohesive.

One of the products of rock weathering is clay minerals and they may accelerate time-dependent deformation of slopes. The distribution of clay minerals depends on the rock type and climate. It was observed that the presence of saturated filling materials in the rock discontinuities lead to wedge failure along the intersection lines of the other discontinuities. In addition, absorption of water by filling materials reduces the friction angle of the failure planes that leading to plane and wedge failures (D. Fereidooni,2018). The shear failure of infilled joints has to overcome the sliding friction of fillings for movement to take place. Direct shear tests showed that the increase of joint undulation enhanced the shear strength of infilled joints and the ratio of filling thickness, t, to the asperity height, a, has a critical value. Below this value, the shear failure strength of infilled joints is higher than the shear strength of fillings and above this value, the shear strength of the infilled joints will be equal to that of the fillings (Wang, Wang, & Zang, 2018). In planar joints, if the particle sizes of the infill material are sufficiently smaller than the infill thickness, such that their movement and rearrangement during shear are not constrained by the joint wall, the thickness of the infill material does not play any significant role on the shear behaviour. Thus, the frictional behavior of the joint would be that of the infill material (Indraratna B., Haque A., 2000)

3.2.4 Groundwater

Groundwater significantly affects geological properties such that the material properties are modified. Recharge sources including precipitation, surface runoff, percolation and nearby wells affect the degree of saturation, hydrostatic head of water and pore water pressures in the surrounding soil. Similarly, the degree of saturation influences the percentage of saturated voids and pore pressure build up thus it is important to understand the ground hydrological processes and their impact. The evaluation of the relationship between properties of the solid rock and water as well as external influences from the excavation process are important. Flowing water widens the discontinuities and causes physical degradation as the porewater pressure induces stresses. The induced stresses and widened discontinuities are responsible for collapse and sliding failure of the rock mass. Groundwater inflow is caused due to precipitation, surface percolation, subsurface leakages and infiltration (Ongodia, J. E., 2017).

Water ingress and drainage mostly in weak discontinuous rock conditions causes swelling and it can be challenging as it is difficult to predict. It is associated with montmorillonite clay minerals of the smectite group such as exist in shale and slate rock discontinuities which has a very high affinity for water causing it to absorb water and expand when saturated through aggregation and flocculation of the clay fabric.

The presence of water in rock discontinuities can lead to a reduction of safety, hydrostatic uplift, sliding and toppling of structures. Movement of water in rock and rock mass happens through available waterways. When flow of water in soil takes place through pores, they are of small significance for the flow process due to their reduced porosity in rocks. Fractures show larger porosity and act as waterways for groundwater in rocks. The aperture, undulation and the type of filling in the fracture regulates its permeability (Gerolymatou E., 2020).

3.2.5 Earth retaining structures

The tunnel is designed to withstand the forces exerted by the retained ground, backfill and other externally applied loads, and to transmit these forces safely to the rock surface. The system is designed to resist lateral earth pressures and water pressures that develop behind the wall. Earth pressures develop primarily because of loads induced by the weight of the backfill and/or retained in-situ soil, earthquake ground motions, and various surcharge loads. For purposes of earth retaining system design, three different types of lateral earth pressure are usually considered: (1) At-rest earth pressure; (2) Active earth pressure; and (3) Passive earth pressure (Zhou Y,2006).

• At-rest earth pressure**:**

It is defined as the lateral earth pressure that exists in level ground for a condition of no lateral deformation. Regarding lateral pressures acting on a retaining structure, movements caused by active pressures are directed away from the soil, and passive resistance pressures which are much larger, could result is movements toward the soil. An intermediate pressure situation must be developed when the structure does not move or strain in either direction. This pressure with zero movement is called earth pressure at rest. (Spangler et al, 1973)

• Active earth pressure:

When horizontal excavation is made in soil, the vertical principal effective stress, σv remains unaltered while the horizontal principal effective stress, σh is reduced because of the removal of the lateral restraint of the soil. This allows the soil structure to expand horizontally until the minimum value of horizontal effective stress is reached and Mohr circle describing the change of stress state touches the failure envelope. This ultimate lower limit of the lateral principal effective stress is called as the 'active earth pressure', pa, and is equal to the product of the coefficient of active earth pressure Ka and σv. Ka is defined as the ratio of pa and σv (Kaul K.,2010). In other words, active pressure is triggered as retained soil moves towards the excavation.

• Passive earth pressure:

If the retained soil were to be pushed away from the excavation a lateral compression of the soil could be caused while leaving the vertical principal effective stress unchanged. This movement results in an increase in lateral pressure relative to the at-rest condition. Further increase in the principal effective stress would lead to a point where the horizontal and the vertical effective stresses would be equal and thereafter grow as the horizontal effective stress exceeding the vertical effective stress until it touches the failure envelope of the compressive Mohr circle describing the change of stress state. This ultimate upper limit of the lateral major principal effective stress is called as the 'passive earth pressure', pp, and equal to the product of the coefficient of passive earth pressure Kp and σv. Kp is defined as the ratio of pp and σv (Kaul K.,2010).

3.2.5.1 Cut-and-cover tunnels

Shallow depth tunnels are generally constructed using the cut and cover technique. For depths up to 15m, this method is often cheaper and practical than underground tunneling. The tunnel is typically designed as a box-shaped frame, and where adequate space is available it is often more economical to use open-cut construction (Wilton J., 1996).

A typical cut-and-cover tunnel construction consist of 4 major stages

*Excavation and ground water control

*Ground support

*Construction of the structure

*Replacement and reinstatement of the backfill

For the construction activity to be carried out safely, the faces of the cut must be properly retained. Excavation in rock for the construction of the structure was carried out inside with an open cut with stabilized side slopes by using wire cutting and blasting. Dewatering is commenced ahead of the excavation at a lead depth of at least 2-3 m for the construction activities to proceed in the dry. The bottom-up method of construction is followed since the road traffic and other major services that existed at the location previously could be safely diverted and the construction of the tunnel begins after placing a filling material of 50cm on the bottom surface. Once the top slab is constructed and waterproofed backfilling can be done in layers to reinstate the ground surface with the replacement of the subgrade and base for the road surface.

3.2.5.1.1 Loads

The tunnel structure should have the structural capacity sufficient to safely resist all loads and influences that may be expected over its life. The loads to be resisted are usually the long-term development of water and earth pressures, dead load including the weight of soil, surface surcharge load, and live load. (Wilton J., 1996).

Gravity loads

Gravity loads comprise of all the loads that act downwards and transmitted to the subgrade below the tunnel. This includes the self-weight of the structure and the weight of the backfill on top of the roof slab. This is calculated as the product of the depth and the unit weight of the constituent section.

Arching

When the ratio of depth of the backfill on top of the tunnel to the width of the tunnel is greater than 0.5 load shedding takes place over the full width of the tunnel due to the downward differential movement of the soil columns outside the shear planes. When the ratio is less than 0.5, the effect is mostly concentrated close to the sides. It is also likely, if at all it does act, to be very small. The width of the excavation and the method of backfilling determines whether the load on the tunnel is likely to experience an increase or decrease. When the structure is constructed within stabilized side slopes, the depth of the backfill on either side of the tunnel is greater than that over the structure. A greater settlement of the deeper backfill on the sides than the combined vertical compression of the structure and that of the backfill directly above it will lead to extra load shedding on to the backfill directly above the structure caused by down drag along shear planes due to negative arching thereby increasing the load on it. When the construction is carried out in an open cut within stabilized side slopes, negative arch action takes place which causes the structure to experience a load which can be in excess of that implied by the actual depth of the soil backfill when the fill outside the longitudinal perimeter walls settles more than the combined total compression experienced by the structure and the settlement of the fill above. Due to the very small magnitude of the aspect ratio, the effect of load enhancement on the structure is considered insignificant and disregarded (Wilton J., 1996).

Traffic surcharge

Where the tunnel is below the road surface, the wheel loads from the vehicular traffic will undergo dispersal with depth and experience a reduction in the intensity before reaching the roof of the tunnel. For depths greater than 600mm the extent of dispersal and the intensity of the surcharge loading likely to act on the roof slab will vary. However, it is assumed that the effect of any downward variation in the surcharge loads at overburden depths greater than 1m is not significant.

Lateral loads

The tunnel which is in intimate contact with the soil on all sides deforms as the stiffness of the surrounding soil and the structure allows it. The lateral loads include horizontal earth pressures and groundwater pressures from the surrounding soil. Below the groundwater table, lateral pressure due to retained soil may be considered as a function of vertical effective stress in the soil. Hence, the soil component of horizontal earth pressure may be small compared with the total horizontal pressure due to both retained soil and retained water. There may be substantial changes to this loading during the life of the tunnel. Soon after construction, the actual short-term earth pressure may be considerably less than long-term design pressure. A future excavation parallel and adjacent to the tunnel can cause unbalanced lateral pressures with a pressure equal to long-term pressure applied to one side and a lesser pressure applied to the other. Whether the structure should be considered restrained against horizontal translation or proportioned for stresses resulting from side sway caused by unbalanced horizontal pressures depends on local requirements. A common recommendation is that the tunnel is proportioned for side sway if it is a single-story structure. The maximum horizontal earth pressure from the soil component should never be taken as less than the product of the vertical effective stress and the coefficient of earth pressure at-rest (Ko). For cohesionless soil, at-rest pressure is computed with the coefficient, Ko equal to 1 – sin(Φ), where Φ equals the effective stress friction angle

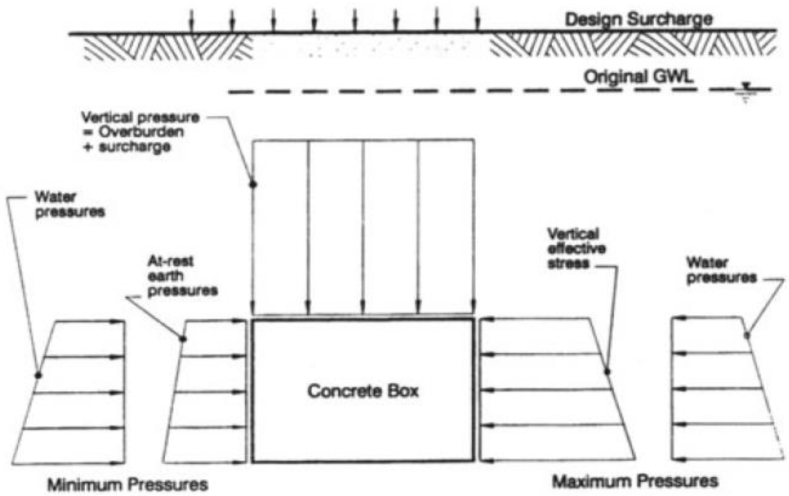

Figure 3.8 Long-term loading on cut-and-cover tunnels (Wilton J., 1996).

When the groundwater table lies above the bottom of the base slab of the structure, an upward pressure on the bottom of the base slab, equal to the piezometric head at that level, must be accounted for. For a rectangular box, this upward pressure multiplied by the width of the base slab is the buoyant force (B) per lineal meter of structure (Wilton J., 1996).

Upward loads

The upward loads acting on the tunnel can be due to the reactive force, heave or the hydrostatic uplift pressure. Terzaghi proposed that bottom pressures would be approximately one-half of the roof load intensity as pressures acting on the roof become more uniformly distributed with increasing depth and their intensity gets reduced proportionately. In addition, the weight of overlying rock mass will tend to increase roof loads but make an opposite effect on bottom pressures. For the derivation of bottom pressures, Tsimbaryevitch assumed that a soil wedge is displaced towards the tunnel cavity due to the action of active earth pressure from the vertical pressure on the lateral parts. The displacement would be resisted by the passive earth pressure on the soil mass under the bottom of the cavity. According to him, the resultant force would be vertical and act at the centre line. This upward pressure could be counteracted either by loading the bottom with the counterweight of intensity like the bottom slab and application of internal ballast or by an invert arch. After the construction of the tunnel, porewater pressures will begin to develop at the base of the structure and continue to rise until the initial hydrostatic conditions are restored. Bottom pressures are usually encountered in loose soils, especially in plastic, saturated clays. In the open tunnel section, the rock at the bottom is not affected by pressure from above to a certain depth. The load from the side rock walls is transferred with its full magnitude to the rock at the bottom and gets distributed over a larger depth with increasing area (K. Szechy,1966).

The gravity loads on the structure which gets transmitted down to the subgrade and a reactive force act on the underside of the tunnel. The self-weight of the tunnel will be lesser than the weight of the rock that which it replaces. In a similar manner, the reactive pressure mobilized will be much less than the overburden pressure experienced at the surface previously. The upward load is calculated by taking the moment of other loads about the center.

Skin friction

If the downward movement of the soil exceeds the combined effect of the settlement and the vertical compression of the structure itself, negative skin friction can occur at the soil–structure interface. In this case, the structure loses the frictional support of the surrounding soil to transfer permanent gravity loads and the surrounding soil could impose additional down-drag forces on the structure leading to further settlements. If the total downward movement of the structure relative to that of the surrounding soil becomes greater, then positive skin friction could occur. This would induce extra loads on the surrounding soil and cause it to settle some more leading to another round of negative skin friction and down-drag loads. This process would continue until soil–structure equilibrium would be reached.

In cohesionless soils such as sands and gravels, due to immediate dissipation, excess porewater pressures do not build up and long-term, drained condition is prevalent. Therefore, it is appropriate that the earth pressures in such soils for long-term design life of the structure are evaluated by an effective stress analysis (Kaul K., 2010).

4

Analytical model

There are different theories for analyzing the lateral ground pressure imposing on a retaining wall or a cut-and-cover tunnel wall. However, in most of them the principle of calculations is based on the Rankine`s and the Coulomb`s theory considering soil pressure behind the wall. In this study, the movement of a rock block along an identified discontinuity has to be considered as well. The first and an important step in developing a reliable analytical model for this case could be identifying and assessment of appropriate loads and forces acting on the concrete tunnel. The forces expected are:

- Driving force caused by the rock movement along the identified discontinuity
- Shear resistance force along the discontinuity
- The effect of the building load on top of the rock block
- Total water pressure force inside the rock discontinuity
- Lateral soil pressure imposed on the wall
- Weight of the filling soil between the wall and rock
- The effect of traffic load on top of the filling soil
- Lateral water pressure
- The reaction force acting on the failure plane inside the backfill

4.1 Rock block failure

The whole cross section of the tunnel and materials surrounding it are illustrated in Figure 4.1. It can be seen that there would be a rock block formed by a discontinuity on the left-hand side of the tunnel. The resultant force caused by the probable rock movement could be obtained by calculating the weight of the block considering load of the building which is located on top of the rock block, water pressure and shear resistance forces. To calculate this, as it is shown in eq.7 its volume per running meter which is the area of the rock block is required. All the parameters used for this step are defined in Table 4.1 below.

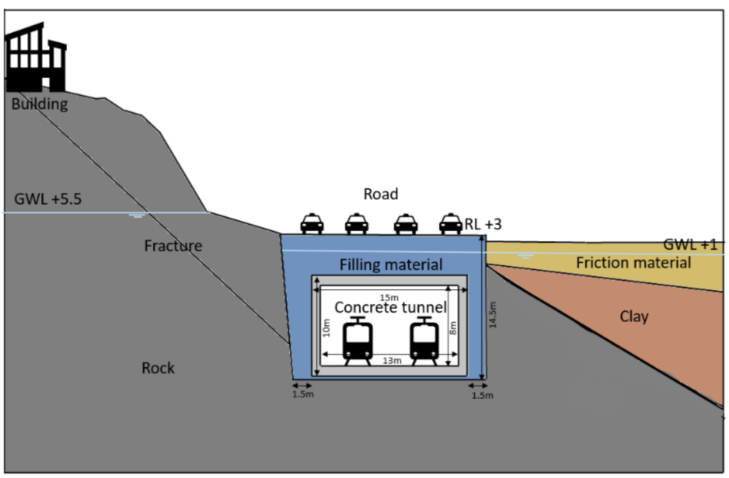

Figure 4.1 Cross-section of the tunnel and its surroundings

Table 4.1 Parameters for calculating resultant force of the rock block

Parameter	Symbol	Unit
Weight of the rock block per running meter	W_r	kN/m
Weight of the rock block plus the building load	W_T	kN/m
Length of the discontinuity	l_v	m
Inner height of the triangle perpendicular to the discontinuity in Figure 4.2	l_b	m
Unit weight of the rock	γ_r	kNm3
Load of the building per running meter	q_b	kN/m
Driving force along the discontinuity	T	kN/m
Shear resistance force	N	kN/m
Angle of the discontinuity	θ	°
Water pressure resultant force	U_r	kN/m
Unit weight of water	γ_w	kN/m3
Height of water level	h_w	m
Length of discontinuity which is filled by water	l_{v-w}	m
Maximum resistance force	T_{r-max}	kN/m
Friction angle of discontinuity infilling	φ	°
Cohesion of discontinuity infilling	c	kN/m^2
The final resultant force by rock movement	E_r	kN/m

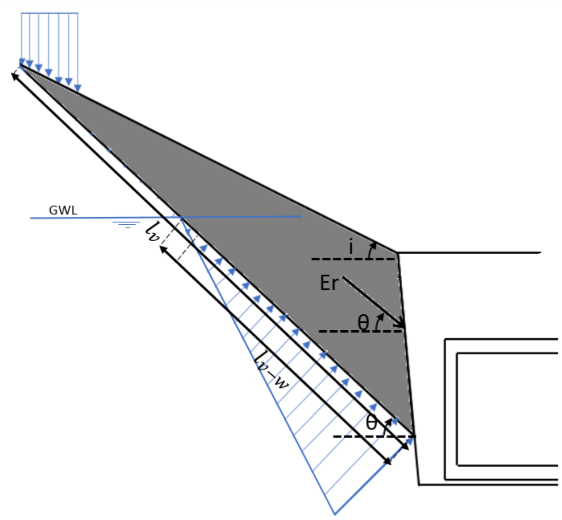

Figure 4.2 Failure mechanism of the rock block

$$W_r = \frac{1}{2} \times l_v \times l_b \times \gamma_r \qquad eq.7$$

To consider the load of the building on top of the rock block, in eq.8 its uniform loading is added up to the weight of the block.

$$W_T = W_r + q_b \qquad eq.8$$

The total weight of the rock block considering the load of the building on the surface has two components, one is tangential force which is the driving force along the discontinuity and is calculated in eq.9.

$$T = W_T \times \sin(\theta) \qquad eq.9$$

The other component would be the normal force which will be used in eq.10 to calculate the shear resistance

$$N = W_T \times \cos(\theta) \qquad eq.10$$

Water could fill the discontinuity up to the water level which is defined in Figure 4.2 and the water pressure resultant force inside the fracture needed to be considered in the resistance force calculations. Then, the maximum resistance force could be calculated by using eq.11 and eq.12.

$$U_r = \frac{1}{2} \times \gamma_w \times h_w \times l_{v-w} \qquad eq.11$$

$$T_{r-max} = \tan(\varphi) \, . (N - U_r) + c. l_v \qquad eq.12$$

The final resultant force caused by the rock block movement parallel to the identified discontinuity could be obtained by subtracting the shear resistance from the driving force as in eq.13.

$$E_r = T - T_{r-max} \qquad eq.13$$

4.2 Soil wedge failure

The next important step in the procedure is analyzing the filling soil gap between the rock and wall and checking how these forces could be conveyed and imposed on the tunnel. As it is mentioned in Chapter 3.1 researchers have studied failure in a narrow backfill behind a retaining wall close to a rock face. In these studies, due to the narrow soil section, the commonly used methods for evaluating forces, such as the method of Coulomb or Rankine, is inappropriate and some other approaches for the failure plane in the backfill are needed to be taken (Greco V ,2013).

Tests implemented by (Woodruff, 2003) on soil sections adjacent to a stable face show that the slip line of the failure is bilinear, including a part inclined at an angle α which is less than the theoretical failure plane of the Rankine theory and the other along the interface between backfill and stabilized wall. These experimental results indicate that traditional methods using the Rankine failure plane to define the active thrusts is not applicable for narrow backfill soils and a specific approach must be applied. Among the various alternative approaches, the limit equilibrium method could be used due to its simplicity in equations (Greco V, 2013). In the limit equilibrium approach, it could be assumed that the rock movement causes a backfill failure along two surfaces (See Figure 4.3), one is (BC), in contact with the wall of concrete tunnel, and the other (AD) in contact with rock face, and (DC) inside the backfill, which can form a thrust wedge ABCD (Chen et al, 2019). Some experimental results on soil models confirm the assumed formation of this failure wedge (Leśniewska et. al, 2001).

The method which is adopted in this study can be considered an extension of Coulomb's theory to evaluate the active thrust exerted by narrow backfill using the limit equilibrium method. It is assumed that the failure wedge is formed by one rigid block, bounded by plane surfaces (See Figure 4.3).

This method has been developed under the following simplifying assumptions (Greco V, 2013):

- The soil obeys the Mohr–Coulomb failure criterion, and it is cohesionless, and without pore pressure.
- There is a lateral movement in the wall of concrete tunnel due to rock movement which is sufficient to induce failure along planes inside the backfill, according to Coulomb's approach.

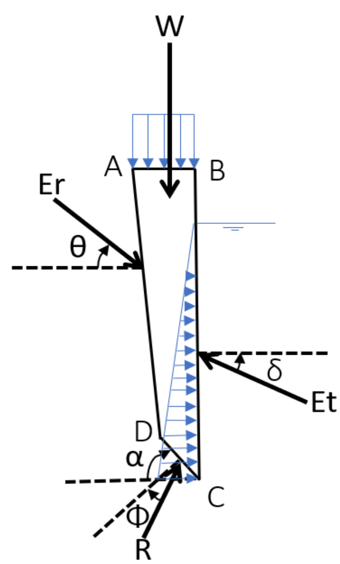

Figure 4.3 Failure wedge of the soil block

To define the forces involved in the backfill soil, a failure mechanism is considered as shown in figure 4.3. In this mechanism, it is assumed that due to the proximity of the tunnel to the rock face, the slip face starts at point C with an angle α to the horizontal and intercepts the rock face at point D, then continuing along the joint line of rock and soil to the top of the soil section. Considering this mechanism, a failure wedge ABCD as in figure 4.3 could be identified. By identifying all the forces acting on the wedge and applying equilibrium equations in both horizontal and vertical directions, the thrust on the tunnel could be achieved. As it can be seen in figure 4.3, this failure wedge is subject to its own weight plus the traffic load on the surface (W), resultant force caused by the rock block movement (E_r) by an angle of θ with the horizontal, the reaction force on the slip plane CD (R) by an angle of ϕ with the normal to the CD, the lateral water pressure on the tunnel (U), and the lateral resultant force on the tunnel (E_t) by an angle of δ with the horizontal. The angle of slip plane (CD) with the horizontal is defined by α in this figure.

The resultant force of the rock block is expected to be applied parallel to the discontinuity, and the angle of resultant force of the tunnel is assumed to be equal to the friction angle between the tunnel and the soil, which could be two third of the soil friction angle based on the Terzaghi's bearing capacity theory (Szechy, 1967). The equation used to calculate the angle of the slip plane in the soil failure wedge was adopted from equation 14. (Greco, V., 2013) All parameters used in this part are defined in Table 4.2.

Table 4.2 Parameters for calculating soil wedge forces

Parameter	Symbol	Unit
The angle of slip plane (CD) with the horizontal	α	°
The angle of reaction force on the slip plane (CD) with the with the normal to the CD	ϕ	°
Angle of the discontinuity or the resultant force of the rock block (E_r) with the horizontal	θ	°
Angle of the lateral resultant force on the tunnel (E_t) with the horizontal	δ	°
Angle of slope on top of the soil	ε	°
Angle of the wall	β	°
Weight of the soil wedge plus the traffic load on the surface	W	kN/m
The resultant force caused by the rock block movement	E_r	kN/m
The reaction force on the slip plane CD	R	kN/m
The lateral water pressure on the tunnel	U	kN/m
The lateral resultant force on the tunnel	E_t	kN/m

$$\alpha = \varphi + tan^{-1}\left(\frac{\sqrt{\frac{\sin(\varphi-\varepsilon)\sin(\beta-\varepsilon)\sin(\varphi+\delta)}{cos^2(\beta-\varphi).\sin(\beta+\delta)}}-\sin(\varphi-\varepsilon)}{\cos(\varphi-\varepsilon)\left[1-\frac{\sin(\beta-\varepsilon)\cot(\beta+\delta)}{\cos(\beta-\varphi)\cos(\varphi-\varepsilon)}\right]}\right) \qquad eq. 14$$

Finally using equilibrium of forces in both x and y directions gives eq.15 and eq.16 to calculate the lateral resultant force on the tunnel and the reaction force on the slip plane.

$$R = \frac{W + E_r.\sin(\theta) - E_t.\sin(\delta)}{\cos(\alpha-\varphi)} \qquad eq. 15$$

$$E_t = \frac{W + E_r \times (\sin(\theta) + \cos(\theta).\cot(\alpha-\varphi)) + U.\cot(\alpha-\varphi)}{\sin(\delta)+\cos(\delta).\cot(\alpha-\varphi)} \qquad eq. 16$$

4.3 Lateral pressure on the right side

To simplify the calculations on the right-hand side of the tunnel, it is assumed that the shear resistance forces caused by the friction between the concrete and soil at the bottom and top of the tunnel are enough to make the whole structure remain in equilibrium. Then the soil on the right side does not undergo any strain or movement. Hence, eq.17 could be used to achieve the 'earth-at-rest' lateral pressure (Kaul, K. ,2010). The value of the coefficient K_0 has some effects on the bending moments acting on the tunnel, which means a higher K_0 leads to higher horizontal stresses leading to higher bending moments and deformations. In this study, the real coefficient of the earth pressure is expected to be larger than K_0, and pressure that is calculated by this coefficient at the right-hand side might be larger (Tjie-Liong, 2014).

$$\sigma_H = K_0(\gamma . z - u_0) + u_0 \qquad eq. 17$$

$$K_0 = 1 - sin\varphi \qquad eq. 18$$

In this equation maximum lateral pressure can be calculated and K_0 is the coefficient of earth-at-rest pressure that can be obtained by a simplified empirical formula, widely accepted for normally consolidated sand (Kaul, K.,2010). Figure 4.4 shows the illustration of lateral pressure on the right-hand side of the tunnel. σ_H is the maximum lateral pressure, and u is the maximum water pressure acting on the tunnel at the right-hand side.

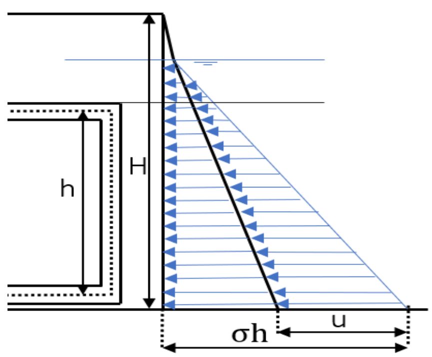

Figure 4.4 Lateral pressure on the right side of the tunnel

4.4 Structural Frame Analysis

Using the adopted method to calculate the pressure at the left side of the tunnel, the 'earth-at-rest' lateral pressure for the right side and knowing the vertical pressure on top of the structure, the vertical distributed reaction on the bottom of the invert slab could be calculated by applying a rigid frame analysis. For that purpose, the commonly accepted methodology was through the consideration of equilibrium of forces acting in the horizontal and vertical direction and moments of forces about the center of the tunnel (Kuesel et al, 2012).

It could be observed that lateral forces acting on the left and right side of the tunnel are not balanced, therefore in this situation, the whole tunnel structure could move to the left. However, there are some resistance forces due to the friction between the concrete and soil at the top and bottom of the tunnel which have to be considered (F1 and F2). This resistance force can be significantly stronger at the bottom interface since it depends on the friction angle between concrete and soil, and the normal force caused by weight of the tunnel and the soil material above it. This difference could lead to larger displacement at the top compared to the bottom. To simplify the calculations, the displacement at the bottom is ignored and it is assumed that the tunnel has fixed supports there and the maximum displacement occurs at top.

The share of the F1 and F2 forces can be defined proportional to the magnitude of the loads acting on the relevant slab.

Using the equilibrium of forces in x and y directions and moments of the forces about the center gives the equations 19, 20, and 21 which can be used to calculate the shear forces (F1 and F2) and the distributed reaction force on the bottom of the invert slab. These forces are illustrated in figure 4.5. Parameters b and d are differences between q_2 and q_1, and q_4 and q_3 respectively.

$$\sum F_x = 0 \quad \rightarrow \qquad F_1 + F_2 = \frac{h}{2}\big((q_1 + q_2) - (q_3 + q_4)\big) \qquad eq.19$$

$$\sum F_y = 0 \quad \rightarrow \qquad q_5 + q_6 = \frac{q_0 \times L + q_R \times L + W_t}{L/2} \qquad eq.20$$

$q_R = uniform\ load\ of\ the\ railway$

$W_t = Total\ weight\ of\ the\ tunnel$

$$\sum M_c \curvearrowleft = 0 \quad \rightarrow \qquad q_6 - q_5 = \frac{-\left((F_1 - F_2) \times {}^{h}/_{2} + (d - b) \times {}^{h^2}/_{12}\right)}{{}^{L^2}/_{12}} \qquad eq.21$$

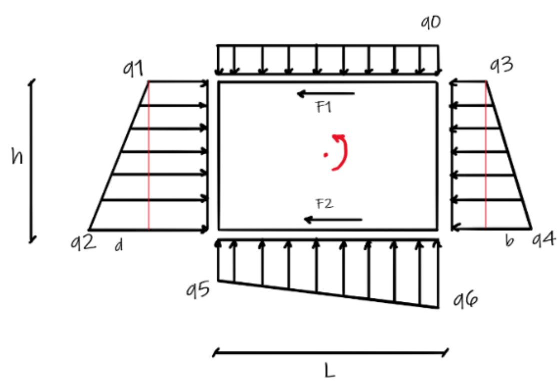

Figure 4.5 Forces acting on the tunnel

4.4.1 Distribution factor method

The distribution factor method considering sway was applied to determine the moments acting on the tunnel. In this method, it is assumed that all joints of the structure are fixed and then fixed end moments are calculated. Since these moments are unbalanced, a balancing moment would be applied which is shared by members meeting at the joints according to their stiffnesses. This balancing moment is called a distributed moment. There is another moment which is used in this method called carryover moment. When a moment is applied to a member, and the point of application is allowed to rotate and the other end is fixed, the additional moment developed at the fixed end is called carryover moment (M'). The cycle of these calculations that are joint balancing, distributing moments among various members and carry overing can be continued until carryover moments are negligible. In following, main equations used in this method are presented. (Bhavikatti, 2013) All the parameters used in this part are defined in table 4.3.

Table 4.3 Parameters in Distribution factor method

Parameter	Symbol	Unit
Stiffness of the member	k	kN.m
Moment	M	kN.m
Slope of point A	θ_A	°
Bending stiffness	EI	kN.m^2
Length of the member	L	m
Carryover moment	M'	kN.m
Sway force	S	kN
Arbitrary sway force	S'	kN
Sway correction factor	k_s	-

As it is mentioned, moments applied on the joint are shared between the members in proportion to their stiffnesses.

$$Stifness, k = \frac{M}{\theta_A} = \frac{4EI}{L} \qquad eq. 22$$

Distribution factor for a member can be defined as the ratio of the stiffness of that member to the sum of the stiffnesses of all the members meeting at the joint.

$$Distribution\ factor = \frac{M_i}{M} = \frac{k_i}{\sum_{i=1}^{4} k_i} \qquad eq. 23$$

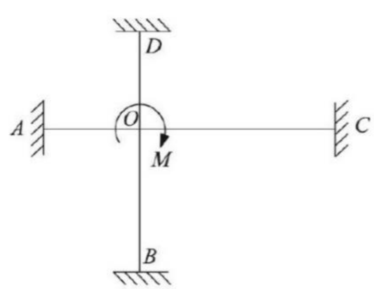

Figure 4.6 Joint subjected to moment M. (Bhavikatti, 2013)

Carryover moment can be defined as:

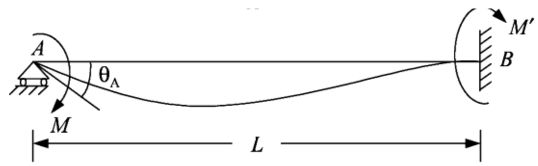

Figure 4.7 Beam with the other end fixed. (Bhavikatti, 2013)

$$Carryover\ factor = \frac{M'}{M} \qquad eq.24$$

$$\frac{ML}{6EI} = \frac{M'L}{3EI} \qquad eq.25$$

$$M' = \frac{M}{2} \qquad Carryover\ factor = \frac{M'}{M} = \frac{1}{2} \qquad eq.26$$

Since there is no symmetry in the loads acting on the tunnel, and horizontal distributed forces acting on it are different on the left and right-hand side of the tunnel, the sway which is the deformation of the structure needs to be considered in the distribution factor method calculations.

First, it can be assumed that the sway is prevented by providing external support at the beam level, then by obtaining the moments based on the distribution factor method and applying the equilibrium of forces in the horizontal direction, a force ‘S’ can be calculated as the force caused by additional support at the beam level.

In the next step, to calculate the sway moments, since the stiffness of both columns is same in this case, then an arbitrary sway force and fixed end moment can be applied for all the joints and the moment distribution method can be applied again. Then by doing the same procedure, sway moments and sway force on the frame can be calculated. Then sway correction factor can be defined as:

$$k\_s = \frac{S}{S'} \qquad eq.27$$

At the end, final moments of each member would be:

$$Final\ moments\ =\ Non-sway\ moments\ +\ k\_s \times\ sway-moments \qquad eq.28$$

4.4.2 Displacement of the tunnel

To obtain the displacement at points B and C in the tunnel, the structure had been simplified by applying two fixed supports at points A and D to calculate the frame deformation. Structural equations 29, 30 and 31 which have been used for this step are shown below. Table 4.4 shows the parameters for these equations.

Table 4.4 Parameters for calculating displacement of the tunnel

Parameter	Symbol	Unit
Displacement by q1	Δ_{q1}	m
Displacement by (q2-q1)	Δ_{q2-q1}	m
Displacement by q3	Δ_{q3}	m
Displacement by (q4-q3)	Δ_{q4-q3}	m
Bending stiffness of the member	EI	kN.m^2
Length of the member	L	m
Displacement at point B (Independently)	Δ_B	m
Displacement at point C (Independently)	Δ_C	m
Total displacement of the frame	Δ	m

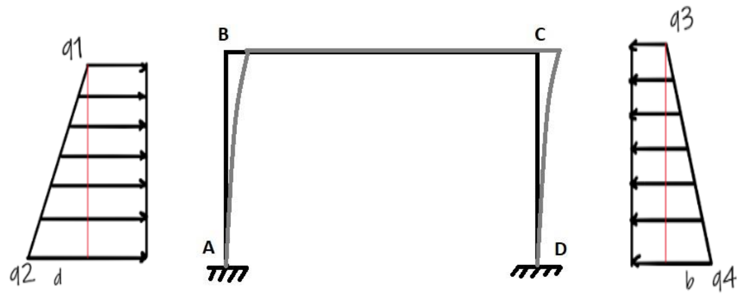

Figure 4.8 Frame deformation

$$\Delta_B = \Delta_{q1} + \Delta_{q2-q1} = \frac{q_1 L^4}{8EI} + \frac{(q_2 - q_1)L^4}{30EI} \qquad eq.29$$

$$\Delta_C = \Delta_{q3} + \Delta_{q4-q3} = \frac{q_3 L^4}{8EI} + \frac{(q_4 - q_3)L^4}{30EI} \qquad eq.30$$

$$\Delta = \Delta_B - \Delta_C \qquad eq.31$$

5

Finite Element model

Modern numerical tools allow complex material behavior and boundary conditions to be taken into account and parametric studies to improve the design are able to be carried out. PLAXIS 2D is an FEM tool that makes it possible to model geotechnical problems either in a plane strain condition or as an axisymmetric model. It governs three main theories in its FEM-code namely: deformation, groundwater flow and consolidation. The general procedure when modelling in PLAXIS is to specify the model type, define the geometry with elements and corresponding materials, define loads and boundary conditions, create a FEM-mesh, define the initial condition, and finally perform the FEM-calculation.

5.1 Units and sign conventions

PLAXIS allows to select a set of basic units for length, force, time, temperature, energy and mass at start of the input of a geometry. The geometry model is created in the x-y plane of the global coordinate system, whereas the positive z-direction is the out-of-plane direction, pointing towards the user. The compressive stresses and forces, including pore pressures, are taken to be negative, whereas tensile stresses and forces are taken to be positive in the output data. Even though PLAXIS 2D is a 2-dimensional program, stresses are based on the 3-dimensional cartesian coordinate system where σzz is taken as the out-of-plane stress in a plane strain analysis.

5.2 Models

It is possible to select from plane strain or axisymmetric models in PLAXIS. A plane strain model is used for geometries with a more or less uniform cross section. Displacements and strains in z-direction are assumed to be zero but the normal stresses in z-direction are fully taken into account. An axisymmetric model is used for structures, circular in shape with a uniform radial cross section and loading around the central axis. The deformation and stress state are assumed to be identical in any radial direction in this model

5.2.1 Mohr-Coulomb model

Failure will occur at a point on any plane in a soil when the shear stress becomes equal to the shear strength at that point. Coulomb suggested a linear equation to calculate shear strength considering parameters including cohesion c, friction angle ϕ, and normal stress at failure. Since only inter-particle forces of a soil can resist the shear stress, the Coulomb function could be expressed using effective stresses, and if the effective stress is zero, then shearing resistance and effective cohesion will be zero as well (Kahlström, 2013).

Based on this equation, a critical combination of these two parameters, shear stress and effective normal stress, will lead to a failure at any point within the soil. Parameters of cohesion and shearing resistance angle are constant values defining a linear relationship between shear strength and effective normal stress (Kahlström, 2013).

To represent a stress state of a 2D soil element in a plot, it is possible to use either a point with coordinates and or a Mohr circle by a major principal stress and a minor principal stress. As it is show in figure 5.1, the envelope of the Mohr-Coulomb failure criterion could be defined as a straight or a slightly curved line touching the Mohr circle or stress points. It is impossible to define a state of stress by a point that is located above the failure envelope, or by a Mohr circle, which is partly above the failure envelope (Craig, 2004).

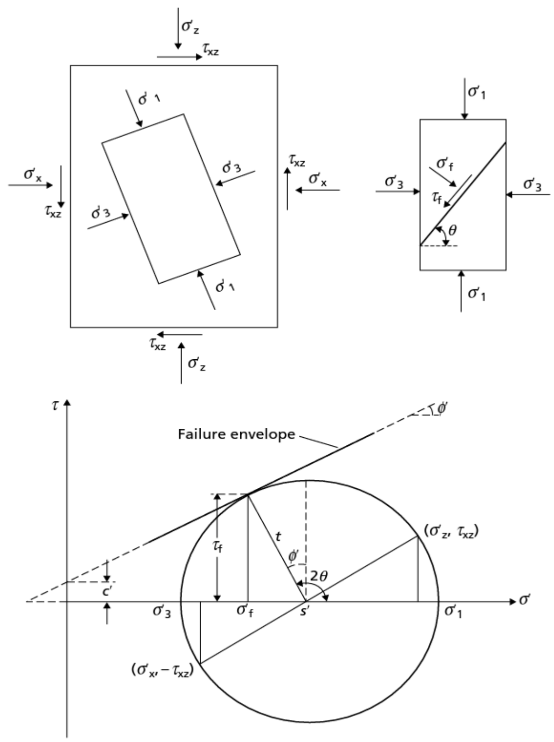

Figure 5.1 Mohr- Coulomb failure criterion (Craig, 2004).

Two of the main characteristics of Mohr-Coulomb model are listed as below (Kahlström, 2013).

- Isotropic linear elastic behavior within the failure surface based on Hook's Law.
- Linear elastic perfectly plastic Failure envelope.

To apply this model five essential input soil parameters are required, and Young's Modulus can be calculated by defining two alternatives.

The main advantages of Mohr-Coulomb model are expressed as below (Kahlström, 2013).

- It is possible to define stiffness by defining two well-known parameters, Young's Modulus and Poisson's ratio.
- Parameters could be obtained easily from different soil tests.
- Reliable results can be achieved within the elastic region.

The main disadvantages of Mohr-Coulomb model could be listed as below (Kahlström, 2013).

- With increasing stress in the basic version of the model, the stiffness remains constant.
- Dilatation is unlimited.
- It includes only ideal-plastic deformations.

When stresses exceed the elastic stress interval, plastic deformations are developed. In the PLAXIS Mohr-Coulomb model, soil stiffness is defined empirically and a linear increment with depth is assumed, while in practice the soil stiffness is dependent on the soil stresses. (Ryltenius, 2011)

Yield functions which are based on principal stresses, friction angle, and cohesion are introduced by PLAXIS to model plasticity. When the material is acting plastic, these functions which can be found in manual PLAXIS (Brinkgreve, 2002) are set to be zero and they make a surface in the principal stress space called the yield surface as shown in figure 5.2. In fact, When the stresses acting on the material are located within this surface, it means that the material is acting elastic, and Hooke's law is valid. (Ryltenius, 2011)

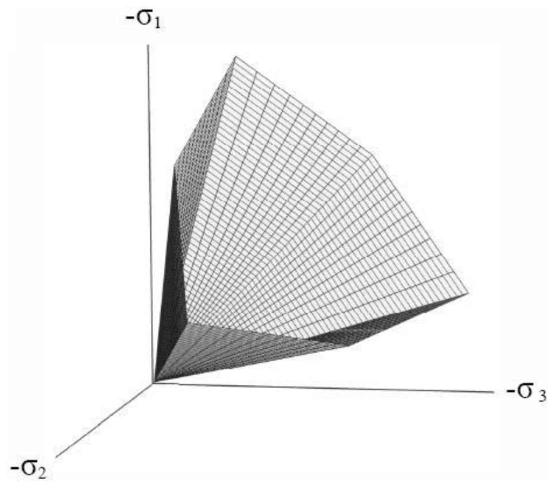

Figure 5.2 Mohr-Coulombs yield surface in principal stress space. (Ryltenius, 2011)

Input Parameters

There are five soil parameters required for the Mohr-Coulomb model to define in PLAXIS. Table 5.1 shows these parameters and their units (Craig, 2004).

Table 5.1 Input parameters of the Mohr-Coulomb model

Parameters		Units
Young's Modulus	E	kN/m^2
Poisson's ratio	υ	-
Cohesion	c	kN/m^2
Friction angle	φ	°
Dilatancy angle	ψ	°

5.2.2 Linear elastic model

The basis of the linear elastic model is the Hooke's law of isotropic elasticity, and two basic elastic parameters are involved in this model including Young's modulus E and Poisson's ratio ν. Linear Elastic model is more suitable to model stiff materials like concrete and intact rock, or strong massive structures in the soil or bedrock layers. But it is not suitable to model soil, since the soil behaviour is highly non-linear and irreversible, and this model is not able to capture these features of soil. Due to the strength of concrete structures, linear elastic model is usually adopted for them. (PLAXIS, 2020)
According to Hooke's law, there are some equations which relate the Young's modulus E and other stiffness moduli, such as the shear modulus G, the bulk modulus K, and the oedometer modulus E_{oed}. These equations can be expressed as below. Input parameters for linear elastic model is shown in Table 5.2.

$$G = \frac{E}{2(1+\nu)} \qquad eq.32$$

$$K = \frac{E}{3(1-2\nu)} \qquad eq.33$$

$$E_{oed} = \frac{(1-\nu)E}{(1-2\nu)(1+\nu)} \qquad eq.34$$

Table 5.2 Input parameters of the Linear elastic model

Parameters		Units
Young's Modulus	E	kN/m^2
Poisson's ratio	υ	-

5.3 Drainage type

Material models in PLAXIS represent the relationship between the stresses and the strains associated with the soil skeleton. The presence of pore water significantly influences the soil response. In order to incorporate the water-skeleton interaction in the soil response the long-term (drained) response or the short-term (undrained) response can be analyzed.

5.3.1 Drained behaviour

In this case, the soil is assumed to be dry or drained fully due to high permeability and/or a low rate of loading. Long-term soil behaviour without generating excess pore pressures and without the need to model the precise history of undrained loading and consolidation can be simulated in this type of setting.

5.3.2 Undrained behaviour

In this case, the soil is assumed to be saturated and that pore water cannot freely flow through the soil skeleton. The clusters in this setting will behave as undrained, even if the cluster or a part of the cluster is located above the phreatic level.

5.4 Geometry and elements

In order to create the required geometry, it is necessary to define points, lines, and clusters. The geometrical clusters are then assigned different material types.

5.4.1 Soil element

There are two different types of elements implemented for soil modelling in PLAXIS 2D and both of them are triangular elements and have either 6 nodes or 15 nodes with 3 and 12 stress points respectively. The element is defined by the choice of the material model assigned to it. One 15-node element can be considered as a combination of four 6-node elements, since the total number of nodes and stress points is equal. The 15-node element provides a fourth order interpolation for displacements and its numerical integration involves twelve stress points while a 6-node triangle provides a second order interpolation for displacements and its numerical integration involves three stress points. This makes one 15-node element more accurate than four 6-node elements and it produces high quality stress results for difficult problems.

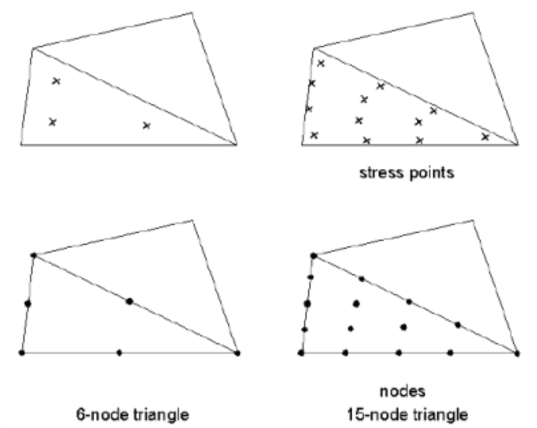

Figure 5.3 6-Noded and 15-noded elements (PLAXIS, 2020).

5.4.2 Interface element

The interaction between two materials can be modelled using interface elements. In a specific node only one displacement is allowed in FEM calculations. Hence, in a node common for two elements with different material properties, the displacement must be the same. Where soil meets structural elements, this is unrealistic, it is expected that the soil to slips and create a gap relative to the structural element. This is solved in PLAXIS by introducing the interface element, which has two nodes for every stress point (Ryltenius A.,2011).

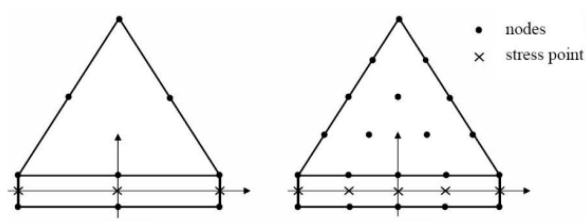

Figure 5.4. Soil element with an interface element for 6-noded and 15-noded elements respectively (PLAXIS, 2020).

Interfaces can be placed at both sides of a geometry lines, enabling a full interaction between structural entities and the surrounding soil. The interfaces are indicated by a plus-sign (+) or a minus sign (-) to distinguish between the two possible interfaces along a geometry line. When connected to a soil element, the interface elements are defined by five pairs of nodes for 15-noded elements, whereas for 6-noded soil elements the interface elements are defined by three pairs of nodes. The interface elements are shown to have a finite thickness in the figure, but in the finite element formulation, each node pair have the same coordinate, which means that the element has a zero thickness. Material properties can be assigned to the interface inorder to simulate interaction between different surfaces. The strength of the interface can be changed with the strength reduction factor Rinter (PLAXIS, 2020).

5.4.2.1 R-inter

There is an important parameter called R-inter in PLAXIS which has to be considered for different materials. In fact, R-inter is the strength reduction factor for the soil-structure interface. Since at interfaces between different soils and structures or stiff materials like intact rock, the soil structure interaction is weaker and more flexible than the surrounding soil, then the reduction factor is applied to consider this matter and can be defined as the ratio of the mobilized shear strength at the soil-structure interface and the shear strength of the adjacent soil. (Kog et al, 2022)
Eq. 36 can describe R-inter in terms of strength parameters: (Wu et al, 2014)

$$Sc = Ss \cdot R\_inter \qquad eq. 35$$

where, Sc is the strength of the contact surface between soil and stiff materials or structures, and Ss is the soil strength around them. When R-inter is equal to 1, it means that there might be no relative displacement between the soil and stiff material and when R-inter is less than 1, then relative displacements can be produced. Therefore, the upper bound value which is 1.0 means that the soil and the structural or stiff component cannot slip one another, and their contact could be considered as rigid. Values less than 1.0 mean that the structural element and the soil mass can slip between one another Wu et al, 2014). Regarding the interface element in PLAXIS, they are used to model the interaction between two materials. In a specific point in FEM calculations, just one displacement can be defined, then in a common node for two materials with different properties, same displacement is presented, which might be not the case where soil and structural elements like concrete or stiff materials like rock have interaction. In this case, an interface element can be introduced which has two nodes for every stress point. The properties of the interface element can be defined by the corresponding soil, and then the strength of the interface could be reduced by assigning values less than 1 to the R-inter factor according to the cohesion and friction angle of the interface element, and this could allow some displacements to be happened there. According to PLAXIS, in most cases, R-inter can be a value of 2/3. Generally, this reduction factor could be greater for cohesive soils than for frictional soils, and it is suggested to be in the range of 0.7-0.8 for cohesive soil and 0.9 for frictional soil (Ryltenius A.,2011).

5.5 Loads

Two types of load definitions are available in PLAXIS, namely distributed load and point load. Since the model is two dimensional, the point load is a one-meter line load in the out-of-plane direction and the distributed load has a thickness of one meter in the out-of-plane direction. The input values of a distributed load are given in the unit of force per length per length of out-of-plane. The default value of a distributed load is one unit in the negative y -direction and if a different magnitude is to be assigned to the absolute load, the program calculates the individual components accordingly, assuming the initial load direction (PLAXIS, 2020).

5.6 Boundary conditions

The finite element method can be used to solve initial and boundary value problems. For the vertical boundaries, the vertical displacement uy is left free and the horizontal displacement ux is restrained. This allows only for a normal stress σ and no shear stress τ. The bottom boundary has total fixities restraining both horizontal and vertical displacements allowing both normal and shear stresses and the restrainment is related to the specific application of the FEM to geotechnical problems. As the depth increases, there is a considerable increase in stiffness of the ground and hence deformation will hardly occur. The upper boundary has no fixities and is left free to displace.

5.7 Mesh generation

The finite element mesh should have a good quality in the sense that the elements should be regular without being excessively long and thin for the numerical stability of the calculation. In areas where significant changes in stress or strain can be expected during the analysis the elements should be small enough for accurate results. The calculation time must also be considered while meshing as an entire mesh of small elements can lead to large computation times. The number of elements generated greatly depends on the shape of the geometry and is not influenced by the element parameters. PLAXIS has an automatic mesh generator which generates a mesh with the chosen type of element, either 6-node or 15- node element. The 15-node elements generate a finer distribution of nodes and hence, accurate results than a similar mesh comprising an equal number of 6-node elements. Five different coarseness of the global mesh are available. The mesh can also be made finer locally in the model, and it helps to ensure sufficient elements in parts exhibiting great stress and strain gradients, without creating a heavy mesh which would consume more time and computer space.

5.8 Defining water conditions

PLAXIS 2D is based on effective stress principles, where total soil stresses are divided into pore pressures in the pores of the soil and effective stresses in the grain skeleton. Groundwater and pore pressures affect the soil behaviour and PLAXIS requires a proper definition of water conditions. Where groundwater flow occurs, the pore pressure distribution may not be known, and a groundwater flow calculation may be required to generate the pore pressures in the soil. A simple hydrostatic pore pressure distribution for the whole geometry can be generated by the global water level. The global water level can be specified for a selected phase, and it also helps to create boundary conditions for the groundwater head when pore pressures are calculated on the basis of a groundwater flow calculation. The FEM calculation can be performed once the geometry is set, and the initial conditions are defined.

5.9 Calculations

In a finite element calculation, when soil plasticity is involved, the problem needs to be solved in a series of calculation steps as the equations become non-linear. A suitable solution algorithm and calculation step size is an important part of the non-linear solution. This reduces the equilibrium errors in the solution and the number of iterations required for equilibrium. A small step size would lead to longer computing times and a large one would lead to a large number of iterations required for equilibrium or diversion of the solution procedure. PLAXIS 2D has an automatic load stepping procedure for solving non-linear plasticity problems and it automatically use the most appropriate procedure to guarantee optimal performance.

5.9.1 Loading type -Staged construction

To resemble and simulate a construction that is built in stages and simulate this, the calculation process in PLAXIS is divided into stages, called calculation phases. The first calculation phase is the initial condition where both the initial effective stress-state and the initial water pressures in the soil are calculated. A number of phases can then be added where structural objects, loads and soil-clusters are activated or deactivated, change of material data and water conditions, according to the planned construction process. In order to specify a new state that is to be reached at the end of the calculation phase, the staged construction loading type is used and it is controlled by the load advancement ultimate level procedure. Modification of the water pressure distribution, the geometry, the input values of loads and the load configuration in the Flow conditions and Staged construction mode can be done accordingly.

5.9.1.1 Generation of initial stress

The initial stresses in soil are affected by the material weight and the history of its formation. In PLAXIS, a calculation type can be defined for a particular phase. For the initial phase, the initial stress state of soil can be generated by the K_0 procedure and Gravity loading. The K_0 procedure is suitable when there is a horizontal surface and all the soil layers and phreatic levels parallel to the surface. It is not recommended for non-horizontal surfaces, which require shear stresses to form an equilibrium stress field. Gravity loading is a type of calculation in which initial stresses are generated based on the volumetric weight of the soil in the first calculation phase.

5.9.1.2 Water pressures

It is possible to generate the initial water pressures in two manners, either directly from the phreatic level or by a steady state groundwater calculation. The definition of the phreatic levels or groundwater head is necessary in these methods. The groundwater calculation is based on the finite element method and the water pressure is calculated by using the permeability of the soil, the generated mesh, and the boundary conditions. The water loads on external model boundaries based on the global water level and steady-state pore pressures are calculated on the basis of the water conditions in active clusters.

5.9.1.3 Plastic calculation

A Plastic calculation carries out an elastic-plastic deformation analysis in which the change of pore pressure with time is not necessary to consider. In a Plastic calculation, the failure and stability of the object are analysed and the loading can be defined by changing the load combination, strength or stiffness of elements, stress state, weight, activated by changing the load and geometry configuration or pore pressure distribution in the staged construction mode. It is used when a change of the model geometry by activation of interfaces is required. In a normal plastic calculation, the stiffness matrix is based on the original undeformed geometry, and this is appropriate in most practical geotechnical applications. Performing a plastic calculation for a fully drained analysis can assess the settlements on the long-term giving a reasonably accurate prediction of the final situation.

There will be some deviation from the exact solution in a non-linear analysis where a finite number of calculation steps are used. A solution algorithm ensures that the equilibrium errors remain within acceptable bounds. Within each step in PLAXIS 2D, the calculation program continues to carry out iterations until the calculated errors are smaller than the specified value the Tolerated error. If the tolerated error is set to a high value, then the calculation would be comparatively quick but may be inaccurate. A low tolerated error on the other hand can make the computer time excessive. By default, it is set to 0.01 and is suitable for most calculations. In a calculation, if the failure loads reduce unexpectedly with increasing displacement, it indicates that there is a deviation of the finite element results from the exact solution. In such a case, the calculation has to be repeated using a lower value of the tolerated error (PLAXIS, 2020).

5.10 The model (Case 1)

The following chapter explains how the software is used to generate the finite element model. The model thus generated is what will be compared to the analytical model and is called Case 1 as several other cases will be simulated in the following chapters. In this study, PLAXIS 2D Version 21 has been used with the plane strain alternative. The 15-node triangle is the default element, and it is used as it is a very accurate element that produces high quality stress results for difficult problems in cases of collapse calculations for incompressible soils (PLAXIS 2022).

5.10.1 Geometry

The FEM model geometry was designed to represent the site condition as close as possible. The width of the model was selected in a manner that the results would not be affected by it. The different elements were created using the soil polygon tool. The polygons for the tunnel was designed having 15m length and 10m height while the walls were 1m thick and was laid 4m below the assumed ground level. Interfaces were defined between these and the surrounding in order to enable a full interaction between tunnel and the surrounding rock and soil. A line was drawn at a depth of 11m from the ground level and at an inclination of 43˚ to the horizontal which would serve as the fracture in the rock. Interface elements were defined on this line as well. Polygons of 1.5m width were defined at the sides of the tunnel to simulate the surrounding filling soil. The soil polygon at the left side of the tunnel was defined at an angle of 83˚ to the horizontal. At the bottom, a soil polygon 0.5m in height was laid to simulate the bed. Two soil section were defined to the right side according to the soil profile of the section. Distributed loads were defined to simulate the traffic load and the building load on top of the rock the loads with magnitudes of 70 kN/m^2 and 22 kN/m^2 respectively. By default, the displacements are prescribed to zero in both x- and y-direction in the bottom and only in the x-direction at the sides and it is followed as such. Since the material at the bottom was completely composed of rock, it was logical not to extend the deformation analysis there.

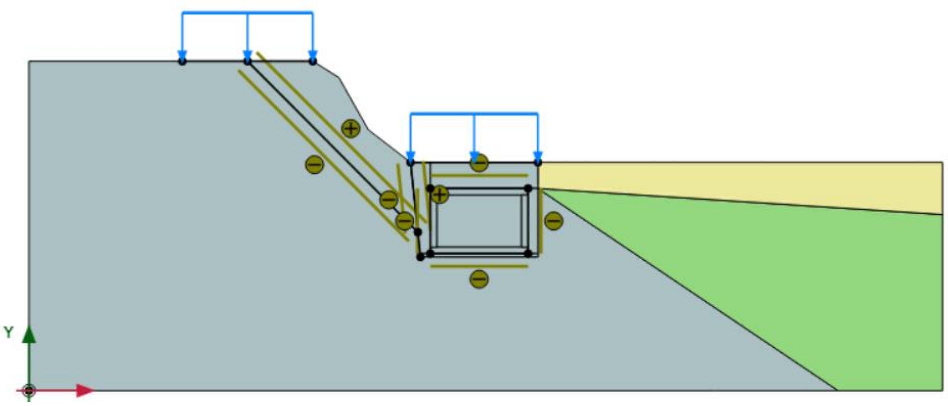

Figure 5.5 Geometry for Case1

5.10.2 Material models and properties

In this study, the Mohr-Coulomb model as the most used model in geotechnics, is chosen for modelling clay, filling, discontinuity infilling, and friction material. Although more advanced constitutive Soft Soil material models, especially when it comes to modeling clay material, could have a better performance comparing to Mohr-Coulomb, due to simplicity and less of parameters needed, Mohr-Coulomb model is applied for these materials. Moreover, Mohr-Coulomb is suggested by PLAXIS manual to use in modelling soils for a first analysis of the problem, since it is relatively fast and fairly accurate (PLAXIS, 2020). Since the objective of this study was to study the effects of the moving rock on the tunnel and the soil gap, the rock could be modelled with the linear elastic model as performed by Rahardjo, P. P and Gong L, et. al. with properties of rock obtained from laboratory test results. Similarly, the concrete was also assigned the linear elastic model with properties of concrete obtained from laboratory test results.

In order to perform the numerical model in PLAXIS, some parameters based on the materials and their relevant models are needed. There is a frictional soil and a clay layer on the right-hand side of the tunnel which are defined in PLAXIS by Mohr-Coulomb models, and the essential parameters are adopted from research, evaluating soil parameters regarding the Göta tunnel project in Gothenburg (Jansson et al, 2006).

Filling material would also be used after the tunnel construction phase to backfill the tunnel. These parameters are shown in the following Table 5.3. Gong L, et. al. used the properties of speswhite kaolin obtained from laboratory results for simulating the properties of infill between rock to investigate their shear behaviour in FLAC 2D. It was modelled as a Mohr- Coulomb material and hence the same is used in this study and named as discontinuity infilling. Regarding the strength reduction factor R-inter, 0.7 is chosen for the discontinuity infilling material, since it has the highest cohesion among the cohesive materials in this case, and 0.8 is assigned to clay on the right side of the tunnel. For filling and friction material, 0.9 is the selected value for R-inter based on the suggestion for frictional soils (Ryltenius A.,2011).

Table 5.3 Material parameters for PLAXIS

Input parameter	Unit	Rock	Concrete	Filling	Clay	Discontinuity Infilling	Friction material
Material model	-	Linear Elastic	Linear Elastic	Mohr-Coulomb	Mohr-Coulomb	Mohr-Coulomb	Mohr-Coulomb
Unsaturated unit weight, γ-unsat	kN/m^3	27.44	24	18	16	15	19
Saturated unit weight, γ-sat	kN/m^3	27.44	24	21	18	18.53	21
Young's modulus, E	kN/m^2	36.23E6	40E6	40E3	50E3	13.94E3	40E3
Poisson's ration, v (nu)	-	0.34	0.15	0.35	0.3	0.2	0.2
Cohesion, c	kN/m^2	-	-	1	1.6	10	0.5
Friction angle, Φ	°	-	-	37	35	17	34
Dilatancy angle, ψ	°	-	-	0	0	0	0.5
Interface reduction factor, R-inter	-	1	1	0.9	0.8	0.7	0.9

5.10.3 Element discretization

Element discretization or the mesh was defined as medium dense and refined well in the tunnel elements and the region in the soil section between the tunnel and sliding rock, as large stress gradients were expected there. The mesh for the model was done as shown in figure 5.6.

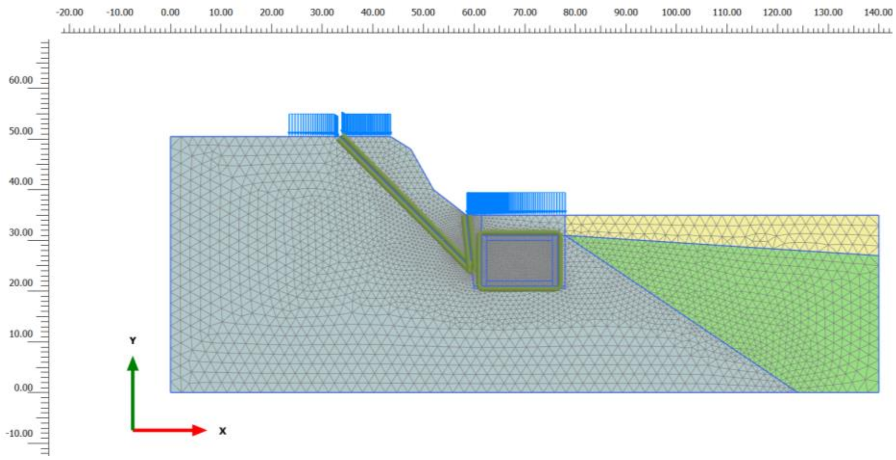

Figure 5.6 Mesh for model Case1

5.10.4 Flow conditions

The global water level was set to y=37.5 m on the left side with the rock and reduced to y=33m where the tunnel starts and towards the right side with respect to the scale shown in figure 5.6. The groundwater flow conditions were set as closed in the sides and the bottom of the model and left open at the top. The pore pressures from clusters involving the hollow tunnel were excluded to simulate the dry environment inside the tunnel.

5.10.5 Staged construction and calculation

Three phases were defined to simulate the staged construction for the model. The initial phase as generated by default with the initial stress development using gravity loading type of calculation. The gravity loading type calculation was used as the layers involved in the model were not horizontal. None of the elements were activated in this phase. A second phase called construction was created where the tunnel was assigned properties of concrete, and the backfilled soil around the tunnel assigned the properties of filling according to Table 5.3. The building load on top of the rock and the traffic load was activated in this phase along with the interfaces around the tunnel. In the final phase named failure, the interfaces in the rock were assigned the material properties of the discontinuity infilling and activated to simulate the rock sliding. Since the phases in the model required change of the model geometry by activation of interfaces, the plastic calculation type was selected and with standard settings for the iterative procedure of phases after the initial phase. In all the phases of the model, the pore pressure calculation type is selected to be phreatic which is based on the input of a global water level and the water conditions of the clusters.

5.10.6 Cases

Table 5.4 Case description

Case No.	**Description**
Case 1	Current model
Case 2	No rock fracture
Case 3	Larger rock block
Case 4	No traffic load
Case 5	Varied discontinuity infilling material
Case 6	Varied R-inter value
Case 7	Varied of water level

Apart from Case 1, a number of models were generated to understand how the results would change with the change in model conditions and parameters. In order to understand the impact of the size of the rock block on the results, two cases were defined, one without any rock movement and another one with a larger rock movement than in Case1. In case 2, the fracture was not defined in the rock mass as shown in figure 5.7 and hence the third phase in the staged construction calculation was avoided. The fracture in the rock mass was defined to be at the toe of the rock slope in case 3, but with the same angle as case 1 as shown in figure 5.8. This was done to displace a larger section of the rock block.

It was also interesting to understand how the results would change in different conditions. Four cases were defined to understand this better. In case 4, the traffic load on top of the tunnel was not considered in this case to understand how much effect it would cause on the stresses and deformation of the tunnel as shown in figure 5.9. This could also create a situation when the tunnel would be newly constructed and before putting into use.

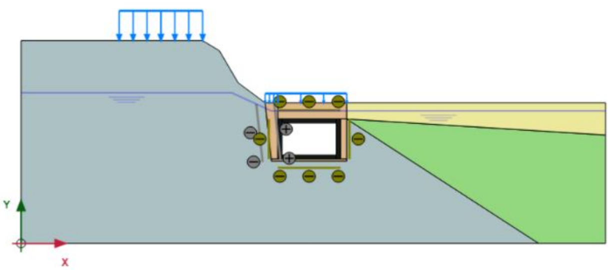

Figure 5.7 Geometry at Failure Phase-Case 2

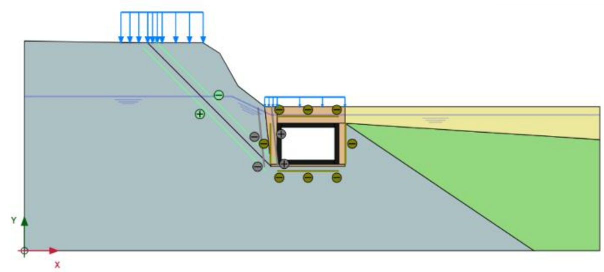

Figure 5.8 Geometry at Failure Phase-Case 3

The interface element was assigned the properties of speswhite kaolin in case 1 and it was interesting to understand what impact the material properties of the discontinuity infilling played a role in the rock movement and the subsequent results. In case 5, the interface at the discontinuity was assigned properties of infilling suggested by Wang X., et.al (2018) which they had used in their simulation of a shear test of rock joint with infilling in FLAC 3D. The numerical model created by Wang et. al. showed a good agreement with the experimental results; hence the model was considered reliable, and its parameters used in this study. A unit weight as in sandy clay was considered with value of 18.5 kN/m^3. The interface reduction factor was considered the same 0.7. The input parameters for the new infilling material is given in table 5.5 and the model is as shown in figure 5.10.

Table 5.5 Input parameters for discontinuity infilling in Case 5

	Model	Elastic Modulus-kN/m^2	Poisson's ratio	Friction angle (°)	Cohesion-kN/m^2
Discontinuity infilling	Mohr-Coulomb	250E3	0.35	25	0.4

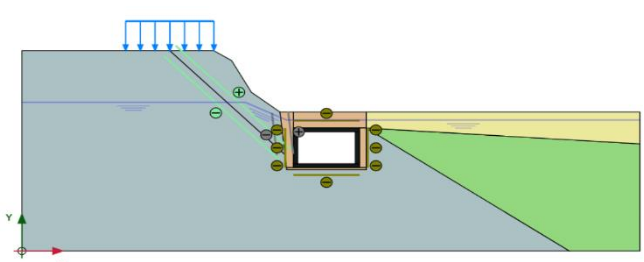

Figure 5.9 Geometry at Failure Phase-Case 4

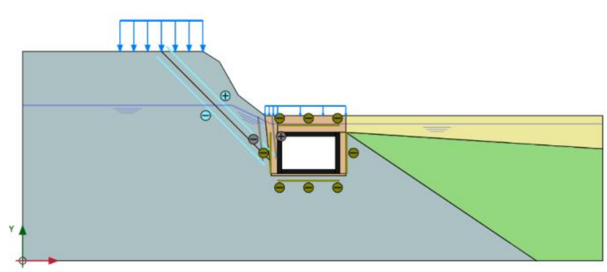

Figure 5.10 Geometry at Failure Phase-Case 5

The value of R-inter assigned to the infilling material at the discontinuity interface was 0.7 for case 1. What impact would make by changing its value was a question of great interest. The value was changed to 0.5 for case 6 to see the changes it made in the model. The model is as shown in figure 5.11. In Case 1, the water level was assigned according to the site conditions and the global water level was defined well above the tunnel. What effect this had on the result was understood by defining a model, case 7 with the global water level defined below the tunnel as shown in figure 5.12.

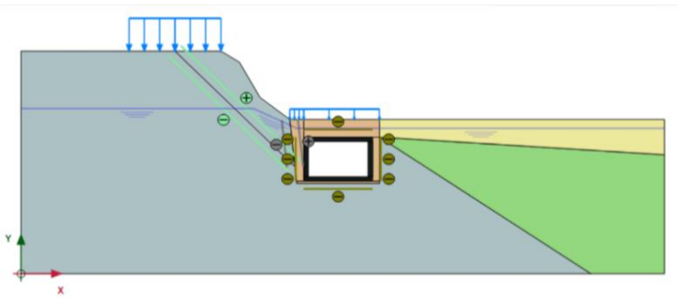

Figure 5.11 Geometry at Failure Phase-Case 6

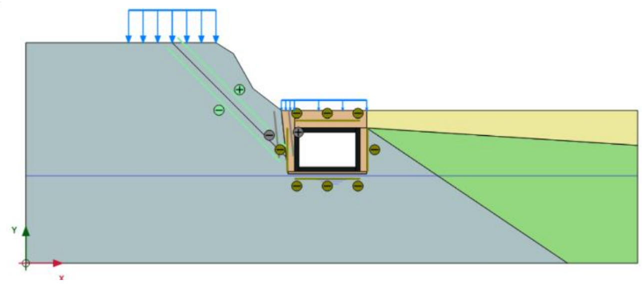

Figure 5.12 Geometry at Failure Phase-Case7

5.10.7 FE Mesh analysis

When the mesh widths are too small, the results will be significantly affected by the displacement boundary conditions. The choice of insufficient mesh widths will cause large settlements as the vertical boundaries will be left free to displace in the vertical direction. Sufficient mesh dimensions have to be considered to avoid the influence of boundary conditions of the results of FE-analysis (Möller S,2006).

However, if the whole rock mass is defined with the same size of elements as the tunnel, a model of large size would be created where the majority of the degrees of freedom are within the rock mass. Moreover, the sections where the rock is not moving is not of interest. Hence, a model with larger elements can be used in the rock further away from the tunnel and finer elements in the tunnel.

The default meshing procedure generated a mesh with a lower density as shown in figure 5.13. This generated only a few elements in the tunnel section. In all the cases, the models were generated after refining mesh in the tunnel and soil junction as shown in figure 5.6. In order to compare the variation in results influenced by the extent of meshing, calculation of the low density meshed model was also done. The results of both models are tabulated in table 5.6.

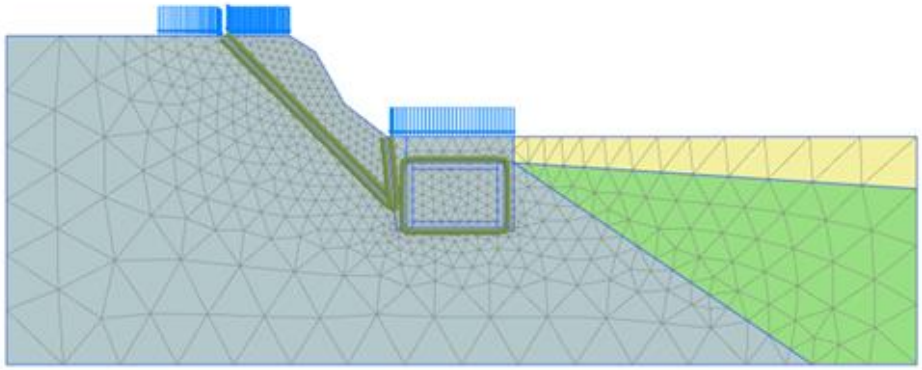

Figure 5.13 Coarse mesh model for mesh analysis

Table 5.6 Comparison of mesh analysis results

	BENDING MOMENT (kNm/m)		SHEAR FORCE (kN/m)		LATERAL DISPLACEMENT Ux, (m)		σ 1-STRESS
	LEFT WALL	RIGHT WALL	LEFT WALL	RIGHT WALL	LEFT WALL	RIGHT WALL	RIGHT WALL
Case	Max	Max	Max	Max	Max	Max	Max
Coarse mesh	1584.53	1295.03	2013.67	1250.90	0.0090	0.00639	11931.37
Refined mesh	1586.28	1306.15	1368.01	1166.21	0.0149	0.0096	27147.03

The models show a significant variation in the results of displacement and stresses. The coarser meshed model shows larger shear forces but lesser displacements and stresses than the refined mesh model for the same conditions. However, the bending moment of both models are close to each other. This shows that with a coarser mesh, PLAXIS underestimates the displacement and stresses in the structural members.

6

Results

6.1 Analytical results

Conducting the analytical calculations based on methods mentioned earlier gives the following results. Distributed forces acting on the tunnel, resistance shear forces at the top and bottom of the tunnel, and the frame displacement value are shown in Table 6.1 below.

Table 6.1 Forces and displacement of the tunnel

Distributed forces (kN/m)	
q0	249.30
q1	186.09
q2	558.27
q3	67.25
q4	179.75
q5	225.86
q6	440.17
Resistance shear forces (kN)	
F1	886.87
F2	2054.27
Frame displacement (m)	0.051

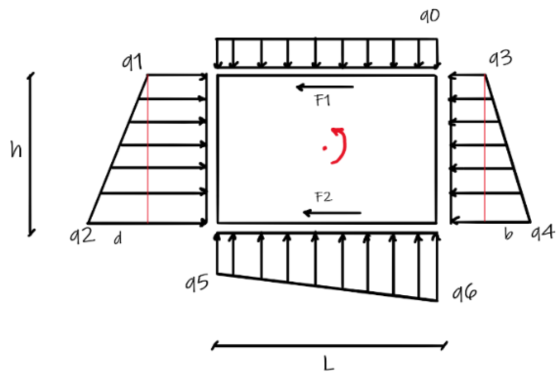

Figure 6.1 Distributed forces acting on the tunnel

The bending moments acting on the tunnel are obtained by the distribution factor method considering sway. Table 6.2 and figures 6.2 and 6.3 below show the results of bending moments and shear force.

Table 6.2 Bending moments

Joint	B		C		D		A	
Member	BA	BC	CB	CD	DC	DA	AD	AB
Bending Moments	3450.39	-3450.39	2464.49	-2464.49	3648.27	-3648.27	4634.16	-4634.16

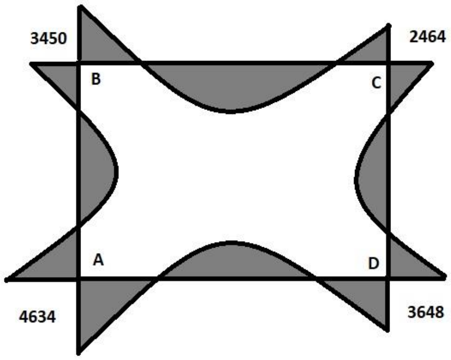

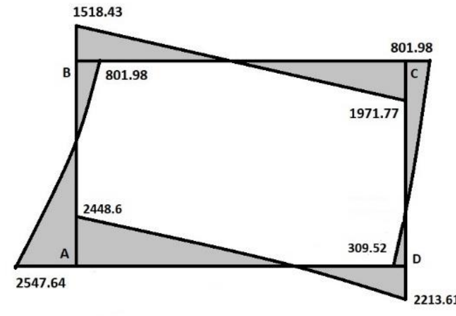

Figure 6.2 Bending moment diagram

Figure 6.3 Shear force diagram

6.2 FEM results

PLAXIS gives the option to show the stress points that are in a plastic state, and it indicates that the stresses lie on the surface of the failure envelope. The failure plane from the rock discontinuity extends into the soil section and the soil fails along the interface between the rock and soil as well, creating a soil wedge. It was observed that the rock block had been displaced in the x direction by 18.5mm.

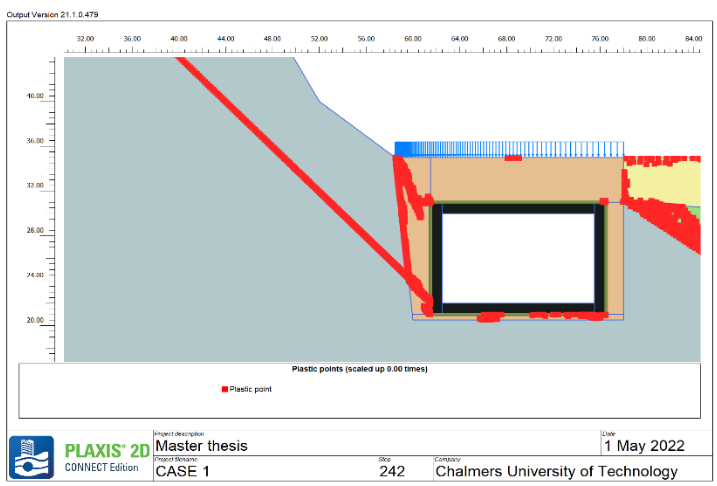

Figure 6.4 Plastic points for Case1

The structural forces in the walls of the tunnel which is composed of volume elements and assigned with concrete properties were visualized by integrating the results in the stress points along the region perpendicular to the cross-section line. The structural forces of interest are bending moment and shear force and their values along the cross-section of the tunnel wall along with their shapes are shown in figure 6.5 and figure 6.6.

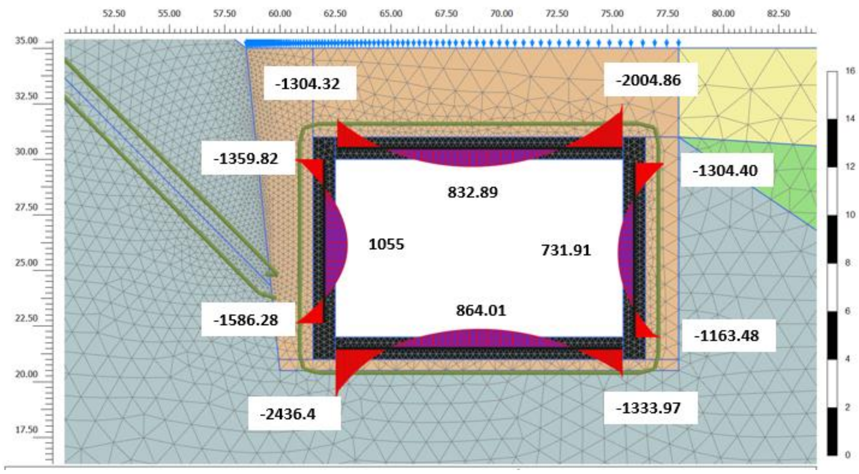

Figure 6.5 Bending moments in the tunnel for Case1

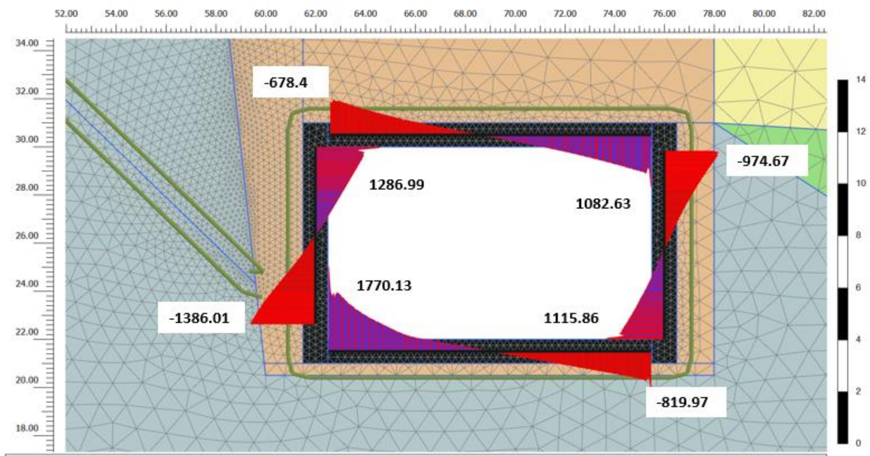

Figure 6.6 Shear forces in the tunnel for Case1

The displacement of the tunnel wall is of great interest as it is a reflection of the impact of the rock movement. As expected, the left and right tunnel walls sways towards the right with a larger deflection on the upper section of the walls as compared to the lower section. The left wall has a maximum deflection of 15mm towards the right whereas the right wall has a maximum deflection of 8mm towards the right as shown in figure 6.7 and figure 6.8.

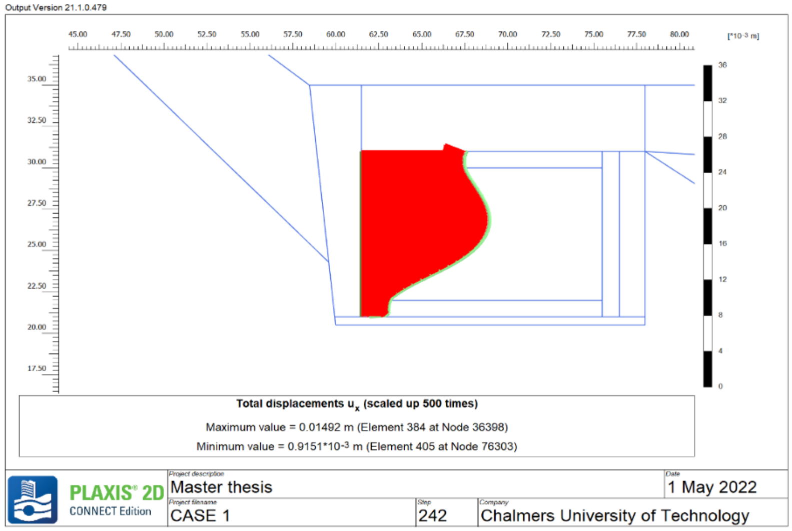

Figure 6.7 Displacement of the tunnel left wall for Case1

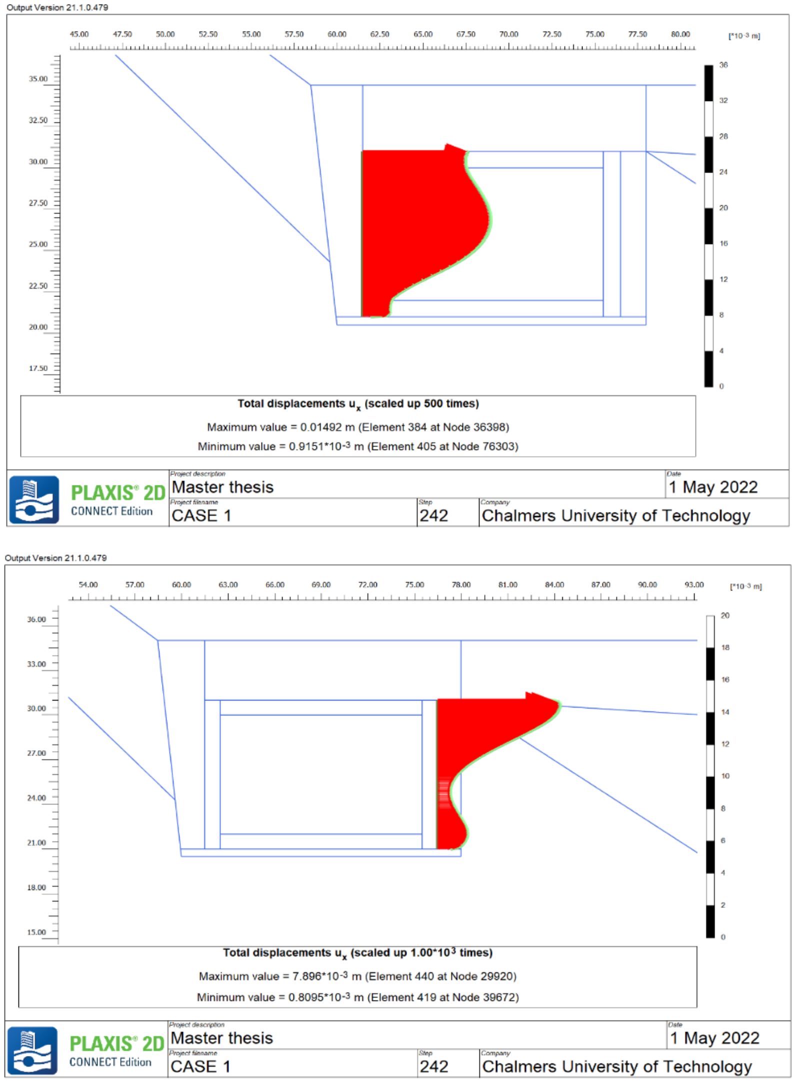

Figure 6.8 Displacement of the tunnel right wall for Case1

Since the placement of the fiber optic measurement system on the right wall should be at the point where there is maximum difference in the stresses, the principal total stresses in the tunnel were observed. The principal total stresses are stress measures based on the sum of effective stresses and active pore pressures, where σ1 is the largest compressive/smallest tension principal stress and σ3 is the smallest compressive/ largest tension principal stress. In order to determine the differential stress, the stresses acting on the tunnel in the construction phase, i.e. before rock movement and the failure phase ie: after rock movement was observed and their difference calculated. This gave the location of the maximum differential stress on the right wall.

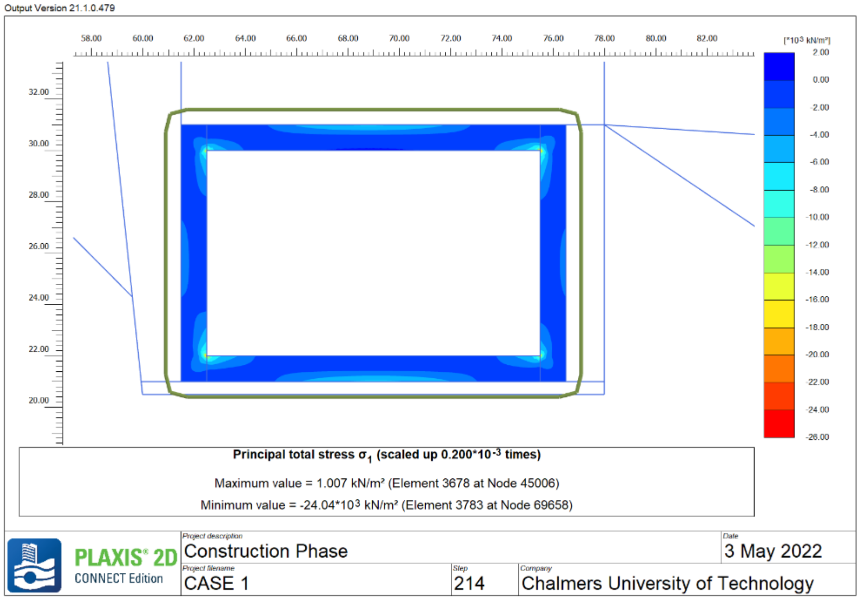

Figure 6.9 Principal total stress in the tunnel for construction phase in Case1

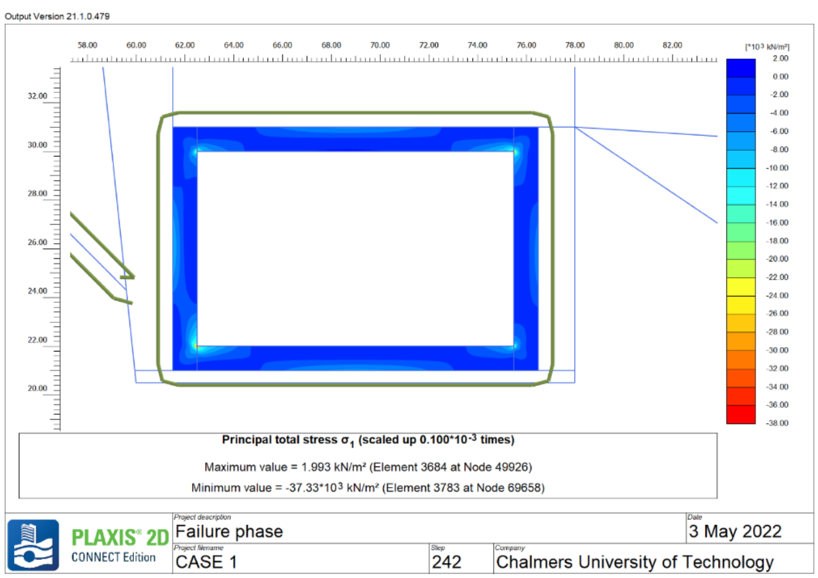

Figure 6.10 Principal total stress in the tunnel for failure phase in Case1

6.2.1 Differential stress

Differential stress of the tunnel with a focus on the right wall is extracted from PLAXIS after observing the principal stresses acting on it at the construction and failure phases and obtaining their difference. To identify the point where the maximum differential stress is acts, MATLAB R2022a software is used to derive the contour map of three variables imported from PLAXIS, which are x coordinates and y coordinates of stress points, and difference of maximum principal stress (σ_1) between the construction and failure phases. This map shows the intensity of the differential stress at different segments of the wall. The general form of this map and coordinates of the point where the maximum differential stress takes place are similar in all studied cases. As it is shown in figure 6.11, the maximum differential stress occurs at a point that is located approximately on the inner corner of the left wall and the upper slab. Table 6.3 shows the values of this maximum stress in different cases. Case 2 has no failure phase; hence the differential stress cannot be accounted for. It can be observed in table 6.3 that in all cases the maximum differential stress is in the range of 4000-5000 kN/m^2, except in case 3 where there is a substantial decrease to around 1700 kN/m^2, and in case 6 where it increases to 5500 kN/m^2.

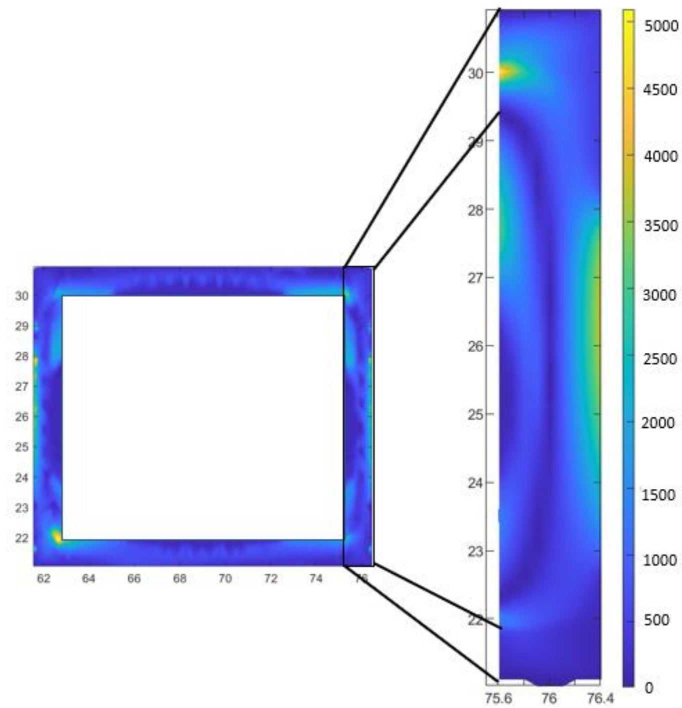

Figure 6.11 Differential stress map for case 1– Right wall of the tunnel

Table 6.3 Maximum differential stresses for different cases

Case	Case 1	Case 3	Case 4	Case 5	Case 6	Case 7
Maximum differential stress (kN/m^2)	4721.56	1693.95	4909.9	4046.08	5552.28	4232.67

The stresses acting on the soil section between the rock and the tunnel was also interesting to investigate. In the construction phase, when there was no pressure from rock sliding, the principal total stress σ1 in the soil was minimum at the surface of the soil section at 21.93 kN/m^2 and reached the maximum value of 634.2 kN/m^2 at the bottom as shown in figure 6.12. Note that PLAXIS uses the negative sign to indicate pressure. At the surface, the stress is contributed only by the traffic load and the increase in stress takes place with increase in the depth of soil.

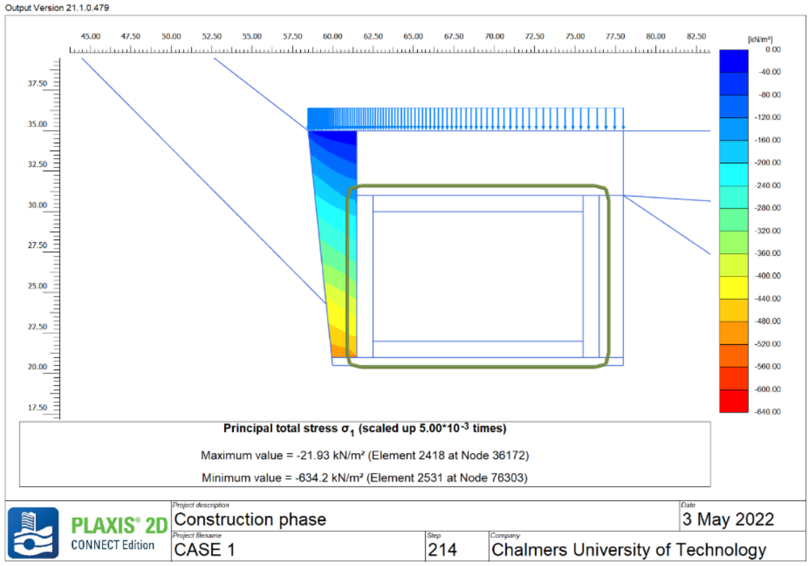

Figure 6.12 Principal total stress in the soil wedge for construction phase in Case1

In the failure phase, the pressure from rock sliding exerted stress on the soil section and the maximum value of principal total stress σ1 was observed where the rock block started sliding into it, reaching a value of 3853 kN/m^2. The minimum value was observed at the soil surface with a value of 27.18 kN/m^2.

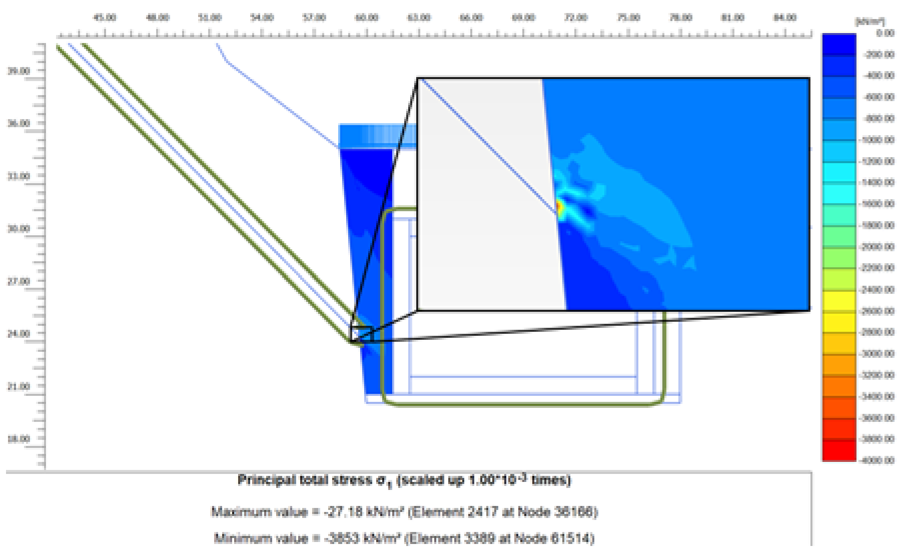

Figure 6.13 Principal total stress in the soil wedge for failure phase in Case1

Earth pressure at rest

Regarding lateral pressures acting on a retaining wall, or in this case, on wall of the tunnel, movements caused by active pressures are directed away from the soil, and passive resistance pressures which are much larger, could result in movements toward the soil. An intermediate pressure situation has to develop when the structure does not move or strain in either direction, and this pressure with zero movement is called earth pressure at rest (Spangler, 1973).

‘Earth at rest’ coefficient K_0

In the analytical model, it is mentioned that the lateral ground pressure at the right-hand side of tunnel is calculated by following the ‘earth at rest’ coefficient as K_0. Using the widely accepted equation to obtain K_0, where the friction angle of the soil is substituted as 37 degrees, gives:

$$K_0 = 1 - sin\varphi = 1 - \sin(37) = 0.4 \qquad eq.36$$

Coefficient of K can be also defined as Rankine’s ratio of lateral pressure to vertical pressure, as it is shown in eq 38 below.

$$K = \frac{\sigma_H}{\sigma_V} \qquad eq.37$$

Using this equation and substituting vertical and lateral pressure at the right-hand side of the tunnel from the numerical model results gives figure 6.14 which is a graph that shows the values of K through the height of the soil column. The variation of K values between 0.4 and 1.6 shows that actual lateral coefficient might be a larger value than K_0.

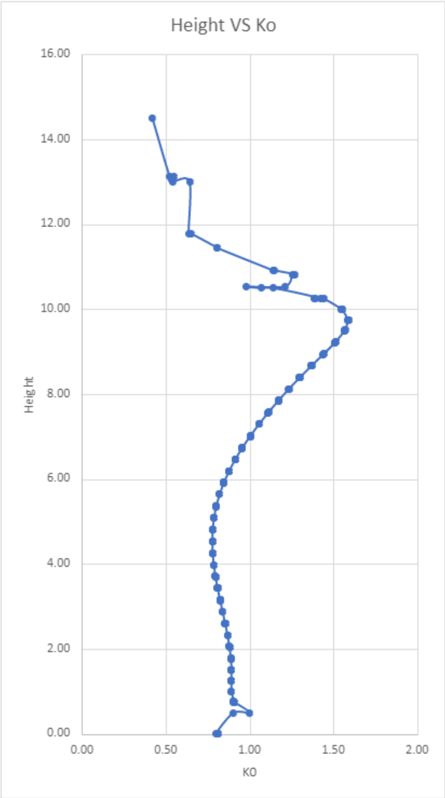

Figure 6.14 Lateral earth pressure coefficient at the right-hand side of the tunnel

6.3 Comparison

6.3.1 Comparison of Analytical and FEM models

As discussed earlier, case 1 is simulated similar to the analytical model and hence the comparison of the analytical model was done by relating it with the FEM results from case 1. The failure points in the model as obtained from PLAXIS is similar to how it was assumed to be in the analytical model, ie: in the form of a wedge.

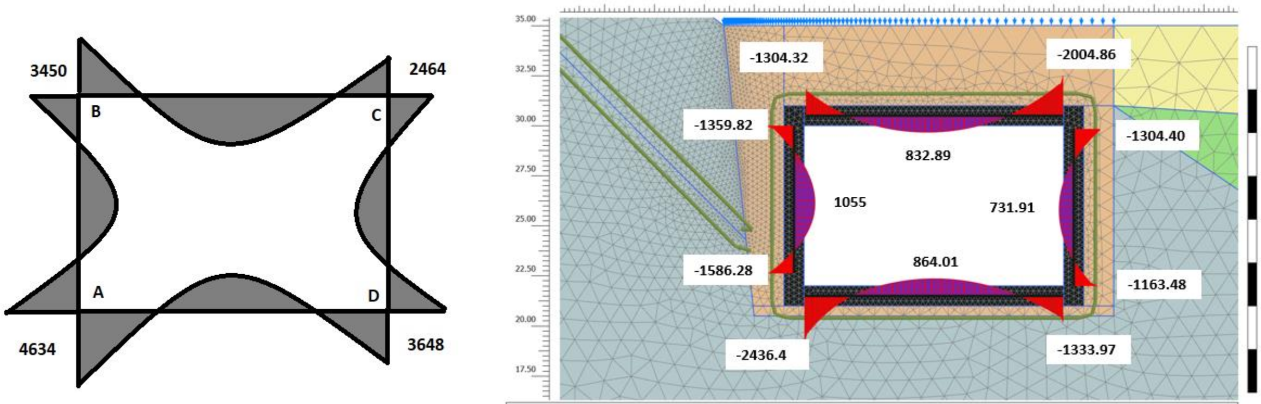

Figure 6.15 Results of bending moments from the analytical and FEM model.

Looking at the bending moment results from the models in figure 6.15, it can be observed that the values at the supports are higher in the analytical model.

Table 6.4 Comparison of analytical and FEM results

	LATERAL DISPLACEMENT Ux(m)	
	LEFT WALL	RIGHT WALL
Case No.	Max	Max
Analytical model	**0.051**	**0.051**
FEM model	**0.015**	**0.008**

The results of the lateral displacement in table 6.4 show as well that the analytical model predicts a higher deflection of the tunnel walls in the same conditions. The numerical analysis takes into account to a wide range of parameters as inputs including cohesion, angle of friction, the introduction of other parameters related to the deformability (E) and the permeability of the soil (k). Analytical methods on the other hand are conservative and overestimate the results. The divergence of results is because the soil between the rock and the tunnel in the analytical model is assumed to be fully plastified and that all the shear resistance it could afford has already been consumed. Whereas the soil shows some resistance in the FEM calculation, hence reducing the amount of horizontal pressure that gets transferred from the rockslide onto the concrete tunnel. This consequently results in higher bending moments and deformations in the analytical model as compared to the FEM model.

6.3.2 Comparison of Case 1,2 and 3

Cases 2 and 3 were defined with no rock movement and a large rock movement in order to understand the impact of rock movement on the structural forces and displacement of the tunnel. The values of maximum bending moment, shear force, lateral displacement, and principal total stress on the tunnel walls are tabulated in table 6.5.

Table 6.5 Comparison table for Cases 1, 2 and 3

	BENDING MOMENT (kNm/m)		Shear force (kN/m)		LATERAL DISPLACEMENT Ux, (m)		σ 1-Stress	ROCK MOVEMENT (m)
	LEFT WALL	RIGHT WALL	LEFT WALL	RIGHT WALL	LEFT WALL	RIGHT WALL	Right wall	Ux
Case No.	Max	Max	Max	Max	Max	Max	Max	
CASE 1	1586.28	1306.15	1368.01	1166.21	0.0149	0.0096	27147.03	0.01856
CASE 2	1479.42	1533.57	1196.89	1060.72	0.0030	0.0023	21445.94	0
CASE 3	1562.05	1256.85	1224.06	1243.42	0.0113	0.0071	25063.99	0.0079

It can be observed that despite a larger rock block movement in case 3, the bending moment and shear forces on the left wall and lateral displacements on both walls are larger for case 1. This can be attributed to the deformation taking place at the midspan of the tunnel wall in case 1 causing a greater deflection and bending moment and in case 3, the deformation taking place at the support of the tunnel causing lesser bending moments and deflection. As expected, the structural forces, stresses and displacements are the least in case 2 as there is no rock movement.

6.3.3 Comparison of Case 1, 4, 5, 6 and 7

In table 6.6 cases 4, 5, 6 and 7 are compared individually with case 1. In case 4, where the traffic load is not considered, the maximum bending moments are slightly decreasing, but the lateral displacement of the tunnel and the rock movement are increases. In case 5, due to the change in the discontinuity infilling material, displacements, bending moments and shear forces are decreased. The reason behind this decrease might be increasing the resistance force of the discontinuity against the rock movement. In case, the important parameter of the infilling discontinuity material which is R-inter has been changed from 0.7 to 0.5. Since this parameter acts as a reduction factor, then this change means more reduction of the interface strength which causes more rock movement. Therefore, as it can be observed, displacements, bending moments and shear forces are increased compared to the case 1. In case 7, the water level is transferred below the tunnel, and this led to some slightly decrease in displacements, bending moments and shear forces.

Table 6.6 Comparison of Cases 1, 4, 5, 6 7.

	BENDING MOMENT(kNm/m)		SHEAR FORCE (kN/m)		LATERAL DISPLACEMENT Ux,(m)		σ 1-STRESS	ROCK MOVEMENT (m)
	LEFT WALL	RIGHT WALL	LEFT WALL	RIGHT WALL	LEFT WALL	RIGHT WALL	RIGHT WALL	Ux
Case No.	Max	Max	Max	Max	Max	Max	Max	
CASE 1	1586.28	1306.15	1368.01	1166.21	0.0149	0.0096	27147.03	0.01856
CASE 4	1543.81	1136.47	1404.85	1187.23	0.0170	0.0106	24203.46	0.02141
CASE 5	1493.61	1290.35	1278.00	1128.63	0.0127	0.0083	26471.18	0.01527
CASE 6	2556.55	1323.08	2007.2453	1220.73	0.0178	0.0113	27974.54	0.02281
CASE 7	1279.16	1269.68	1140.17	950.33	0.0121	0.0087	25474.38	0.01608

7

Discussion

In the analytical calculations, the concrete tunnel is assumed to move away from the rock slope on its left-hand side. On its right-hand side, the tunnel wall is assumed to be at rest, and hence the pressure is calculated using the coefficient of earth pressure at rest. In reality, there is a movement of the tunnel towards the soil section at the right-hand side which leads to the condition of passive earth pressure. Assuming passive earth pressure on the right-hand side would generate passive pressures, which are of greater magnitudes than the pressure exerted by the forces on the left-hand side. This would result in the deception that the tunnel would move towards the rock slope which is not likely. Hence the value of value of K, should be in between the coefficient of earth pressure at rest and the passive earth pressure. Analytical calculation of the exact condition is more complex and hence avoided. This results in the value of deformation obtained from analytical model to be greater than it is supposed to be, ie:51mm. In the finite element calculations for Case 1, on deriving the coefficient of earth pressure from the total horizontal and vertical stresses at the interface between the soil and concrete tunnel, the K value varied from 0.4 to 1.6. Using the average of these numbers ie: K=1 for back analysing the deflection in the tunnel with the analytical model would give 20 mm deflection. This is more in line with the FEM results.

The simulation of discontinuities as discrete elements is performed using the interfaces' function and assigning the material to it. The latest version of PLAXIS, V 22 allowed the user to model the discontinuity using a discontinuity element which work as an independent feature and act as a separate cluster with their own material and water condition. The discontinuity element function would simulate the situation better than how the current model would with the interface function.

In the analytical model, the angle of the slip plane in the soil failure wedge α was observed to be 52° while the angle made by the discontinuity with the horizontal θ was 43°. The finite element model showed that the failure line in the soil was extended from the discontinuity having almost similar angles.

The Rinter parameter specified in the material properties played a major role in simulating the rock sliding. When assuming the that the interface strength is rigid, there is no movement observed in the rock and it requires its strength needs to be brought down in order to simulate the rock sliding.

Since the model simulates the rock deformations with magnitudes comparable to that in nature and the results obtained are in a way relatable to the analytical model, it is considered reliable. Results from such a reliable model could be used in infrastructure projects to get an insight of the stress distributions and deformations that would occur.

The maximum differential stress on the right-hand side of the concrete tunnel was observed to be at the junction between the upper wall and the right wall. This position was observed to be the same in all the simulated cases even though the magnitude of the differential stress varied over a significant range. Hence the positioning of the deflection measurement device could be assured to be there.

8

Conclusion

To answer the research questions of this study, two models have been generated; the first one being the analytical model based on an extension of Rankine theory. In this model, for the left-hand side of the tunnel the soil in the gap between the tunnel and rock is assumed to be failure. The equilibrium of forces is used to analyse the forces acting here whereas the lateral coefficient at-rest pressure is used for the right-hand side. The second one was the numerical model developed in PLAXIS 2D by using the Mohr-Coulomb model for infilling material and soil layers and linear elastic model for concrete and rock. Different cases were generated to see how much the results will be changed in different conditions.

As an important conclusion, apart from case 2 which has no rock movement, the determined discontinuity led to a considerable rock movement and both tunnel walls deflected to the right side with larger magnitudes on the upper section of the walls as compared to the lower section.

Differential stress map with a focus on the right wall illustrated that the maximum differential stress occurs at the inner edge and the highest point of the wall below the upper slab. This would be the location where the fiber optic measurement device could be installed to monitor the maximum effects of the rock movement on the tunnel.

Comparison between the results of the analytical model and the numerical model showed that in the PLAXIS model there are some failure points in the soil gap between the rock and tunnel, roughly similar to what has been assumed in the analytical model as the failure plane. However, the values of moments and lateral deformations obtained by the analytical model are higher than by the numerical model, considering that analytical methods are generally conservative. The other reason behind this difference could be related to how the stresses are transferred through the soil the gap. In the analytical model, the soil is assumed to be fully plastified and all the forces are conveyed to the tunnel without any resistance, while in PLAXIS, and probably in reality there would be still some resistant forces inside the soil. Moreover, the lateral pressure coefficient which is used in the analytical calculations of the right-hand tunnel wall is considered to be at-rest-pressure. While looking through the “K” values derived by PLAXIS it was seen that the lateral coefficient assumed in the analytical model should be larger than K_0, and this would lead to lesser displacement towards of the wall.

References

Bhavikatti, S. S. (2013). Structural analysis-II. Vikas Publishing House.

Chen, F., Lin, Y., & Li, D. (2019). Solution to active earth pressure of narrow cohesionless backfill against rigid retaining walls under translation mode. Soils and Foundations, 59(1), 151-161.

Craig, R. F. (2004). Craig’s soil mechanics. CRC press.

Ongodia, J. E. (2017). Geotechnical engineering design of a tunnel support system-a case study of Karuma (600MW) hydropower project (Master's thesis, University of Cape Town).

Fereidooni, D. (2018). Influence of discontinuities and clay minerals in their filling materials on the instability of rock slopes. Geomechanics and Geoengineering, 13(1), 11-21.

Gerolymatou E. (2020). Notes for rock mechanics, Chalmers University of Technology.

Gong, L., Nemcik, J., & Ren, T. X. (2018). Numerical simulation of the shear behavior of rock joints filled with unsaturated soil.

Greco, V. (2013). Active thrust on retaining walls of narrow backfill width. Computers and Geotechnics, 50, 66-78.

Indraratna B., Haque A., (2000), Shear behavior of clean rock joint. Shear behavior of rock joints, 17-51.

Jansson, A., & Wikström, J. (2006). Load Effects on Permanent Diaphragm Walls. Interaction between soil and concrete structure (Master's thesis).

Johnson, C. E., Grisso, R. D., Nichols, T. A., & Bailey, A. C. (1987). Shear measurement for agricultural soils—A review. Transactions of the ASAE, 30(4), 935-0938.

Kahlström, M. (2013). PLAXIS 2D comparison of Mohr-Coulomb and soft soil material models.

Kaul, K. (2010). Cut-and-cover metro structures: geo-structural design: an integrated approach. CRC Press.

Kuesel, T. R., King, E. H., & Bickel, J. O. (2012). Tunnel engineering handbook. Springer Science & Business Media.

Kog, Y. C., & Loh, K. K. (2022). Soil Parameters of Kallang Formation and Old Alluvium in Singapore for Excavation Study with PLAXIS. Practice Periodical on Structural Design and Construction, 27(2), 04022006.

Leijon, B. (1993). Mechanical properties of fracture zones (No. SKB-TR--93-19). Swedish Nuclear Fuel and Waste Management Co.

Leśniewska, D., & Mróz, Z. (2001). Study of evolution of shear band systems in sand retained by flexible wall. International journal for numerical and analytical methods in geomechanics, 25(9), 909-932.

Möller, S. C. (2006). Tunnel induced settlements and structural forces in linings (pp. 108-125). Stuttgart, Germany: Univ. Stuttgart, Inst. f. Geotechnik.

Plaxis, B. V. (2018). Plaxis 2D reference manual. The Netherlands.

Priest, S. D. (1993). Discontinuity analysis for rock engineering. Springer Science & Business Media.

Rahardjo, P. P. (n.d). USE OF INTERFACE ELEMENT FOR SIMULATION OF BRECCIA RESLIDING ON CLAYSTONE. Parahyangan Catholic University, Bandung, Indonesia.

R. B. J. Brinkgreve (2002): *PLAXIS 2D Version 8*. User manual. A.A. Balkema Publishers, Netherlands, 2002.

SGI (2012). Landslide risks in the Göta River valley in a changing climate. The Göta River investigation Final report, Part 2 Order Photos on the cover Swedish Geotechnical Institute (SGI) SE-581 93 Linköping, Sweden

Spangler, M. G., & Handy, R. L. (1973). Soil engineering (No. 624.151 S6 1973).
Tjie-Liong, G. (2014). Common mistakes on the application of PLAXIS 2D in analyzing excavation problems. International Journal of Applied Engineering Research, 9(21), 8291-8311.

Szechy, K. (1967). The art of tunnelling, Akademiai Kiado Budapest.

Trafikverket. (2021, 05 27). Trafikverket. From www.trafikverket.se: https://bransch.trafikverket.se/en/startpage/projects/Railway-construction-projects/The-West-Link-ProjectVastlanken/The-stations-and-the-tunnel/

Trafikverket (Director). (2022). Västlänken på 1 minut [Video].

Wang, X., Wang, R., & Zang, Z. (2018). Numerical Analysis Method of Shear Properties of Infilled Joints under Constant Normal Stiffness Condition.

Wilton, J. L. (1996). Cut-and-Cover Tunnel Structures-Tunnel engineering handbook. Kluwer academic pulishers.

Woodruff R. Centrifuge modeling of MSE-shoring composite walls. Master thesis, Department of Civil Engineering, The University of Colorado, Boulder; 2003.

Wu, J. J., Cheng, Q. G., Liang, X., & Cao, J. L. (2014). Stability analysis of a high loess slope reinforced by the combination system of soil nails and stabilization piles. Frontiers of Structural and Civil Engineering, 8(3), 252-259.

Zhou, Y. (2006). Geotechnical Engineering: Earth Retaining Structures,. Department of Transportation, Federal Highway Administration

Appendix

1. Analytical Results

1.1 Rock block failure results

Parameter	Symbol	Unit	Result
Weight of the rock block per running meter	W_r	kN/m	5489.92
Load of the building per running meter	q_b	kN/m	2520
Weight of the rock block plus the building load	W	kN/m	8009.92
Length of the discontinuity	l_v	M	37.11
See Figure 4.2	l_b	M	7.25
Area of the block	A	m^2	200.07
Unit weight of the rock	γ_r	kN/m3	27.44
Driving force along the discontinuity caused by rock block weight and load of the building on top	T	kN/m	5460.52
Shear resistance force considering weight of the rock block and load of the building on top	N	kN/m	5860.16
Angle of the discontinuity	θ	°	43
Water pressure resultant force	U_r	kN/m	1232.88
Unit weight of water	γ_w	kN/m^3	10
Height of water level	h_w	m	13.2
Length of discontinuity which is filled by water	l_{v-w}	m	18.68
Maximum resistance force considering water pressure	T_{r-max}	kN/m	1600.74
Friction angle of discontinuity infilling	φ	°	17
Cohesion of discontinuity infilling	c	kN/m^2	10
The final resultant force by rock movement	E_r	kN/m	3859.78

1.2 Soil wedge forces results

Parameter	Symbol	Unit	Result
The angle of slip plane (CD) with the horizontal	α	°	52.05
The angle of reaction force on the slip plane (CD) with the with the normal to the CD	ϕ	°	37
Angle of the discontinuity or the resultant force of the rock block (E_r) with the horizontal	θ	°	43
Angle of the lateral resultant force on the tunnel (E_t) with the horizontal	δ	°	20
Angle of slope on top of the soil	ε	°	0
Angle of the wall	β	°	90
Weight of the soil wedge plus the traffic load on the surface	W	kN/m	735.54
The resultant force caused by the rock block movement	E_r	kN/m	3859.78
The reaction force on the slip plane CD	R	kN/m	1959.79
The lateral water pressure on the tunnel	U	kN/m	720
The lateral resultant force on the tunnel	E_t	kN/m	4312.43

1.3 Distribution factor method results

Joint	B		C		D		A	
Member	BA	BC	CB	CD	DC	DA	AD	AB
Length	9.00	14.00	14.00	9.00	9.00	14.00	14.00	9.00
Moment of Inertia	0.0833	0.0833	0.0833	0.0833	0.0833	0.0833	0.0833	0.0833
Distrib. Factor	0.61	0.39	0.39	0.61	0.61	0.39	0.39	0.61
FEM	2260.99	-4071.93	4071.93	-757.68	909.55	-5789.30	5089.22	-2763.44
Distribution	1102.31	708.63	-1296.88	-2017.37	2970.28	1909.47	-910.09	-1415.69
Carry Over	-707.85	-648.44	354.31	1485.14	-1008.68	-455.04	954.73	551.15
Distribution	825.57	530.72	-719.79	-1119.67	890.96	572.76	-589.26	-916.63
Carry Over	-458.31	-359.89	265.36	445.48	-559.83	-294.63	286.38	412.78
Distribution	498.04	320.17	-278.16	-432.69	520.11	334.36	-273.59	-425.58
Carry Over	-212.79	-139.08	160.08	260.05	-216.34	-136.79	167.18	249.02
Distribution	214.18	137.69	-164.40	-255.74	214.95	138.18	-162.86	-253.34
Carry Over	-126.67	-82.20	68.84	107.48	-127.87	-81.43	69.09	107.09
Distribution	127.14	81.73	-68.99	-107.33	127.40	81.90	-68.94	-107.24

Carry Over	-53.62	-34.50	40.87	63.70	-53.66	-34.47	40.95	63.57
Distribution	53.64	34.48	-40.92	-63.65	53.65	34.49	-40.90	-63.62
Carry Over	-31.81	-20.46	17.24	26.82	-31.82	-20.45	17.24	26.82
Distribution	31.82	20.45	-17.24	-26.82	31.82	20.45	-17.24	-26.82
Carry Over	-13.41	-8.62	10.23	15.91	-13.41	-8.62	10.23	15.91
Distribution	13.41	8.62	-10.23	-15.91	13.41	8.62	-10.23	-15.91
Carry Over	-7.95	-5.11	4.31	6.71	-7.95	-5.11	4.31	6.71
Distribution	7.95	5.11	-4.31	-6.71	7.95	5.11	-4.31	-6.71
Carry Over	-3.35	-2.16	2.56	3.98	-3.35	-2.16	2.56	3.98
Distribution	3.35	2.16	-2.56	-3.98	3.35	2.16	-2.56	-3.98
Carry Over	-1.99	-1.28	1.08	1.68	-1.99	-1.28	1.08	1.68
Distribution	1.99	1.28	-1.08	-1.68	1.99	1.28	-1.08	-1.68
Carry Over	-0.84	-0.54	0.64	0.99	-0.84	-0.54	0.64	0.99
Distribution	0.84	0.54	-0.64	-0.99	0.84	0.54	-0.64	-0.99
Carry Over	-0.50	-0.32	0.27	0.42	-0.50	-0.32	0.27	0.42
Distribution	0.50	0.32	-0.27	-0.42	0.50	0.32	-0.27	-0.42
Carry Over	-0.21	-0.13	0.16	0.25	-0.21	-0.13	0.16	0.25
Distribution	0.21	0.13	-0.16	-0.25	0.21	0.13	-0.16	-0.25
Carry Over	-0.12	-0.08	0.07	0.10	-0.12	-0.08	0.07	0.10
Distribution	0.12	0.08	-0.07	-0.10	0.12	0.08	-0.07	-0.10
Carry Over	-0.05	-0.03	0.04	0.06	-0.05	-0.03	0.04	0.06
Distribution	0.05	0.03	-0.04	-0.06	0.05	0.03	-0.04	-0.06
Moment Sum	3522.63	-3522.63	2392.26	-2392.26	3720.51	-3720.51	4561.92	-4561.92

1.4 Sway moments and final moments

Joint	B		C		D		A	
Member	BA	BC	CB	CD	DC	DA	AD	AB
Length	9.00	14.00	14.00	9.00	9.00	14.00	14.00	9.00
Moment of Inertia	0.0833	0.0833	0.0833	0.0833	0.0833	0.0833	0.0833	0.0833
Distrib. Factor	0.61	0.39	0.39	0.61	0.61	0.39	0.39	0.61
FEM	-100.00	0.00	0.00	-100.00	-100.00	0.00	0.00	-100.00
Distribution	60.87	39.13	39.13	60.87	60.87	39.13	39.13	60.87
Carry Over	30.43	19.57	19.57	30.43	30.43	19.57	19.57	30.43
Distribution	-30.43	-19.57	-19.57	-30.43	-30.43	-19.57	-19.57	-30.43
Carry Over	-15.22	-9.78	-9.78	-15.22	-15.22	-9.78	-9.78	-15.22
Distribution	15.22	9.78	9.78	15.22	15.22	9.78	9.78	15.22
Carry Over	7.61	4.89	4.89	7.61	7.61	4.89	4.89	7.61
Distribution	-7.61	-4.89	-4.89	-7.61	-7.61	-4.89	-4.89	-7.61

Carry Over	-3.80	-2.45	-2.45	-3.80	-3.80	-2.45	-2.45	-3.80
Distribution	3.80	2.45	2.45	3.80	3.80	2.45	2.45	3.80
Carry Over	1.90	1.22	1.22	1.90	1.90	1.22	1.22	1.90
Distribution	-1.90	-1.22	-1.22	-1.90	-1.90	-1.22	-1.22	-1.90
Carry Over	-0.95	-0.61	-0.61	-0.95	-0.95	-0.61	-0.61	-0.95
Distribution	0.95	0.61	0.61	0.95	0.95	0.61	0.61	0.95
Carry Over	0.48	0.31	0.31	0.48	0.48	0.31	0.31	0.48
Distribution	-0.48	-0.31	-0.31	-0.48	-0.48	-0.31	-0.31	-0.48
Carry Over	-0.24	-0.15	-0.15	-0.24	-0.24	-0.15	-0.15	-0.24
Distribution	0.24	0.15	0.15	0.24	0.24	0.15	0.15	0.24
Carry Over	0.12	0.08	0.08	0.12	0.12	0.08	0.08	0.12
Distribution	-0.12	-0.08	-0.08	-0.12	-0.12	-0.08	-0.08	-0.12
Carry Over	-0.06	-0.04	-0.04	-0.06	-0.06	-0.04	-0.04	-0.06
Distribution	0.06	0.04	0.04	0.06	0.06	0.04	0.04	0.06
Carry Over	0.03	0.02	0.02	0.03	0.03	0.02	0.02	0.03
Distribution	-0.03	-0.02	-0.02	-0.03	-0.03	-0.02	-0.02	-0.03
Carry Over	-0.01	-0.01	-0.01	-0.01	-0.01	-0.01	-0.01	-0.01
Distribution	0.01	0.01	0.01	0.01	0.01	0.01	0.01	0.01
Carry Over	0.01	0.00	0.00	0.01	0.01	0.00	0.00	0.01
Distribution	-0.01	0.00	0.00	-0.01	-0.01	0.00	0.00	-0.01
Carry Over	0.00	0.00	0.00	0.00	0.00	0.00	0.00	0.00
Distribution	0.00	0.00	0.00	0.00	0.00	0.00	0.00	0.00
Carry Over	0.00	0.00	0.00	0.00	0.00	0.00	0.00	0.00
Distribution	0.00	0.00	0.00	0.00	0.00	0.00	0.00	0.00
Moment Sum	-39.13	39.13	39.13	-39.13	-39.13	39.13	39.13	-39.13
ACTUAL SWAY moment	-72.23	72.23	72.23	-72.23	-72.23	72.23	72.23	-72.23
ACTUAL SWAY+ NON-SWAY	3450.39	-3450.39	2464.49	-2464.49	3648.27	-3648.27	4634.16	-4634.16

2 FEM Results

2.1 Case 2

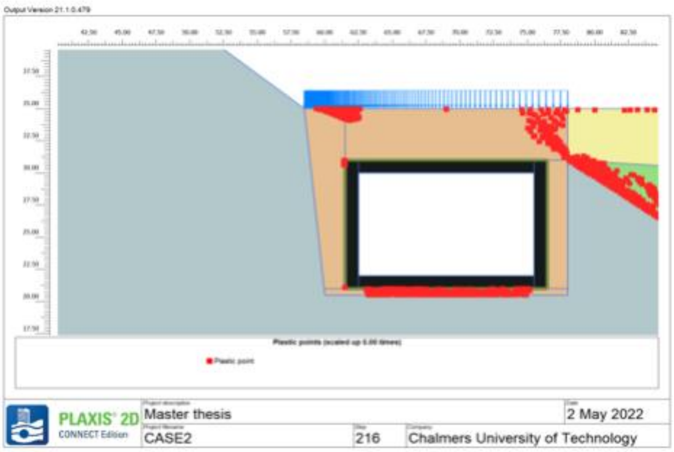

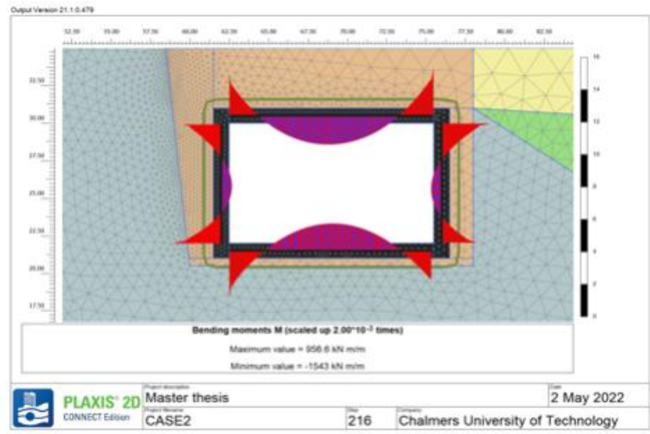

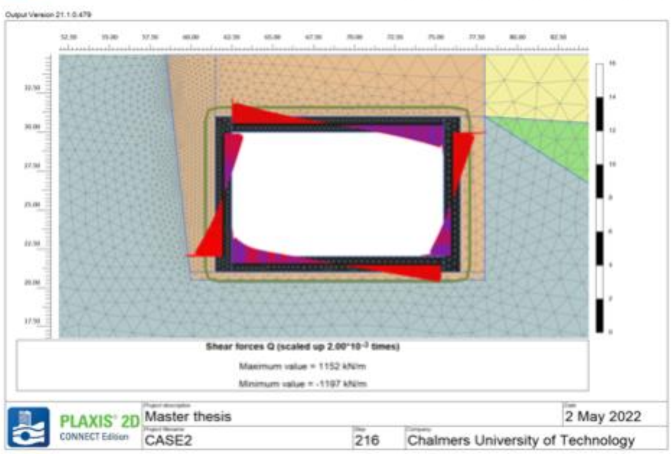

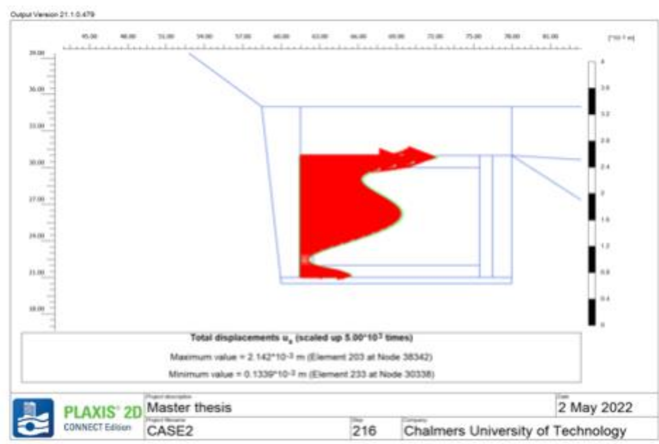

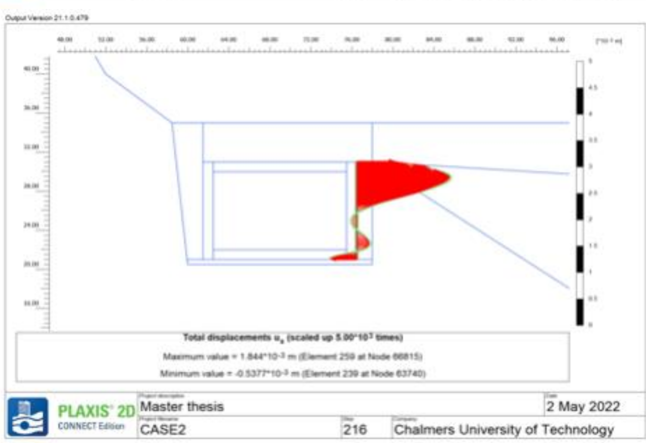

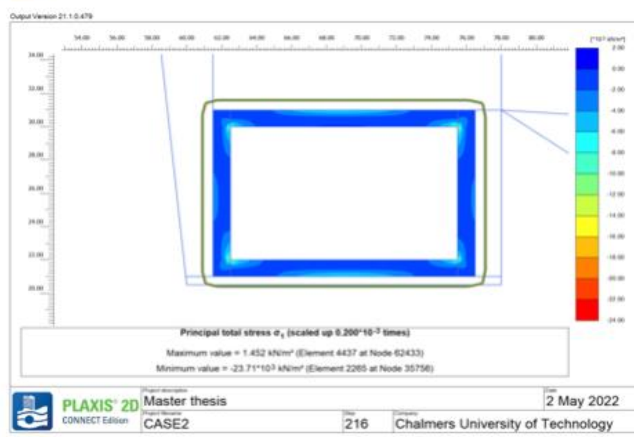

2.2 Case 3

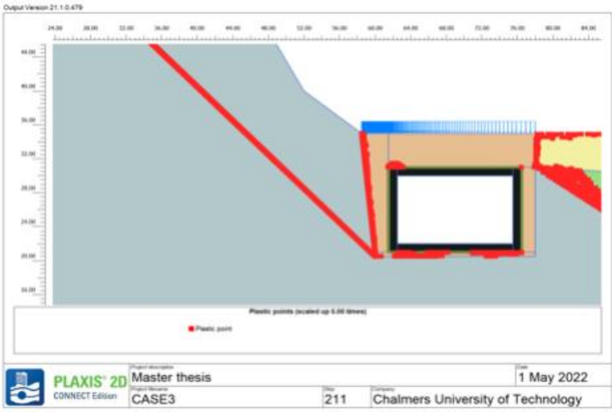
PLAXIS 2D
CONNECT Edition
Master thesis
1 May 2022
CASE3
211
Chalmers University of Technology

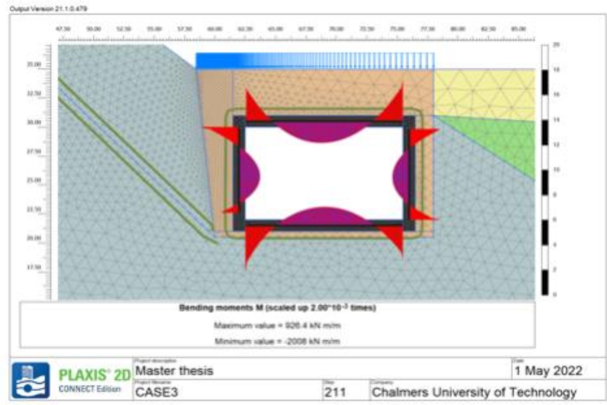
PLAXIS 2D
CONNECT Edition
Master thesis
1 May 2022
CASE3
211
Chalmers University of Technology

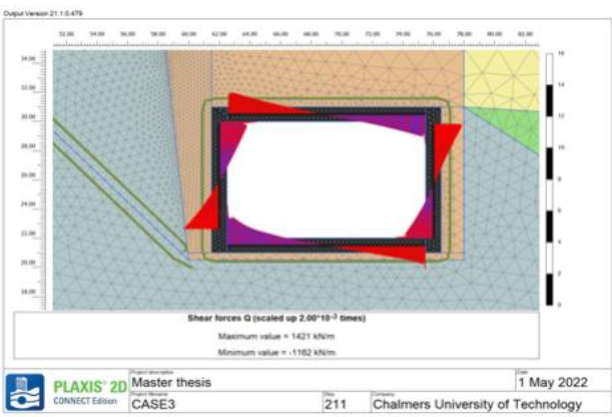
PLAXIS 2D
CONNECT Edition
Master thesis
1 May 2022
CASE3
211
Chalmers University of Technology

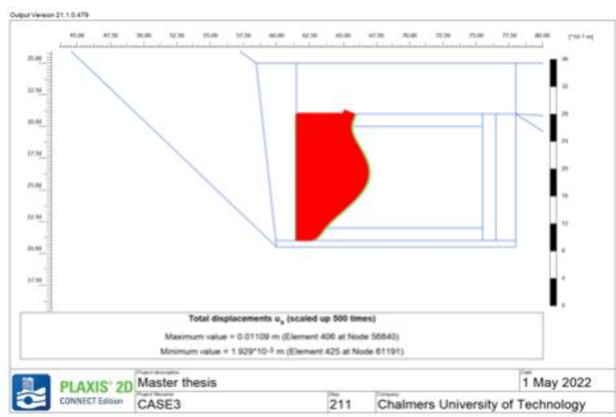
PLAXIS 2D
CONNECT Edition
Master thesis
1 May 2022
CASE3
211
Chalmers University of Technology

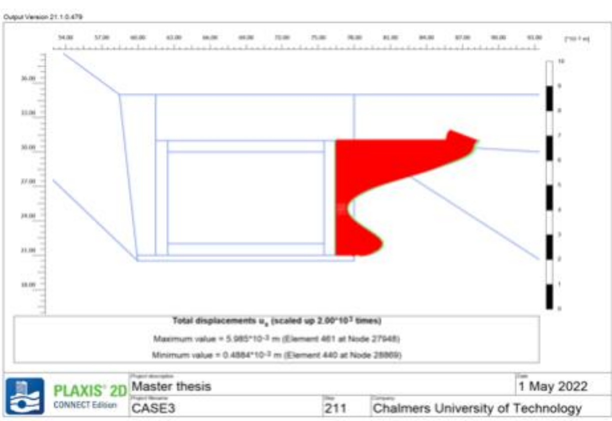
PLAXIS 2D
CONNECT Edition
Master thesis
1 May 2022
CASE3
211
Chalmers University of Technology

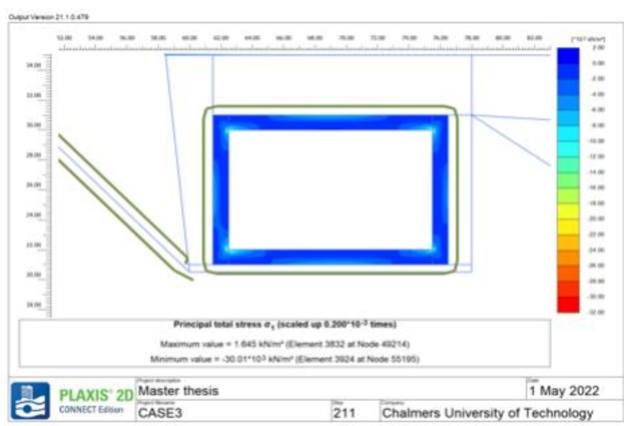
PLAXIS 2D
CONNECT Edition
Master thesis
1 May 2022
CASE3
211
Chalmers University of Technology

2.3 Case 4


Plastic points (scaled up 5.00 times)
Plastic point
PLAXIS 2D
CONNECT Edition
Master thesis
1 May 2022
CASE 4
250
Chalmers University of Technology

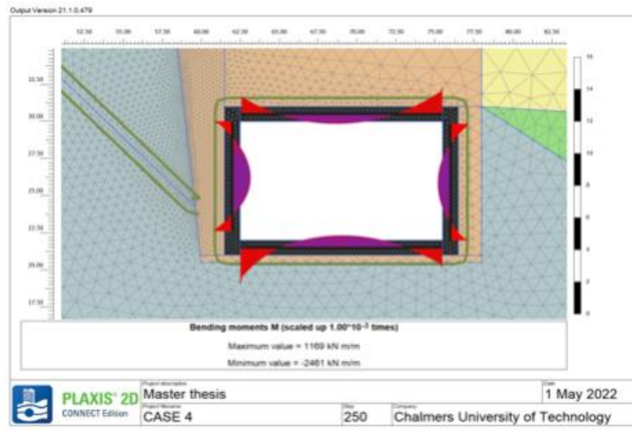
Bending moments M (scaled up 1.00*10^-3 times)
Maximum value = 1169 kN m/m
Minimum value = -2461 kN m/m
PLAXIS 2D
CONNECT Edition
Master thesis
1 May 2022
CASE 4
250
Chalmers University of Technology

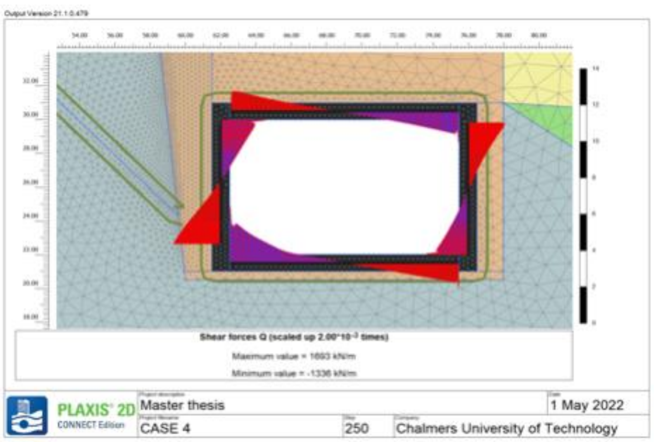
Shear forces Q (scaled up 2.00*10^-3 times)
Maximum value = 1693 kN/m
Minimum value = -1336 kN/m
PLAXIS 2D
CONNECT Edition
Master thesis
1 May 2022
CASE 4
250
Chalmers University of Technology

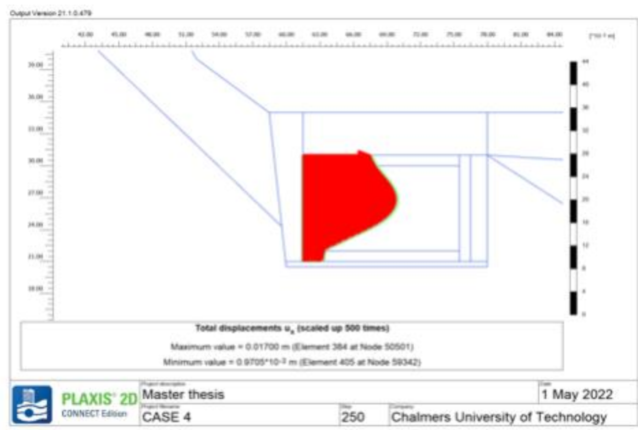
Total displacements u (scaled up 500 times)
PLAXIS 2D
CONNECT Edition
Master thesis
1 May 2022
CASE 4
250
Chalmers University of Technology

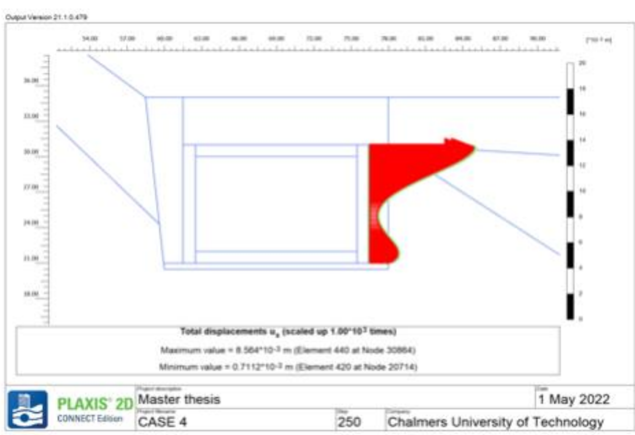
Total displacements u
PLAXIS 2D
CONNECT Edition
Master thesis
1 May 2022
CASE 4
250
Chalmers University of Technology

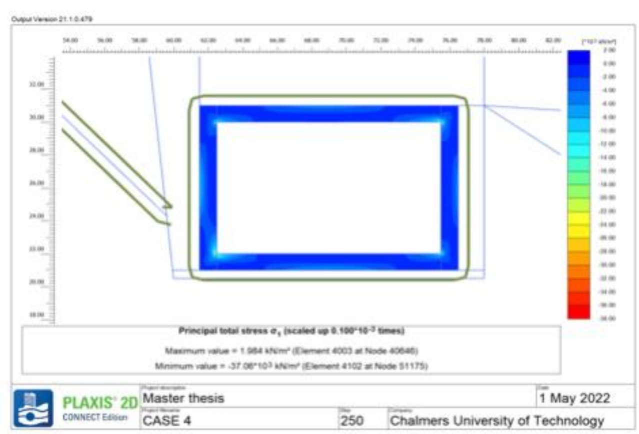
Principal total stress σ
PLAXIS 2D
CONNECT Edition
Master thesis
1 May 2022
CASE 4
250
Chalmers University of Technology

2.4 Case 5

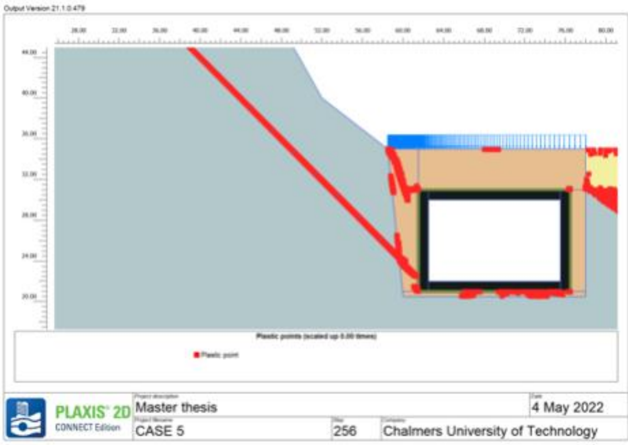
PLAXIS 2D
CONNECT Edition
Master thesis
4 May 2022
CASE 5
256
Chalmers University of Technology

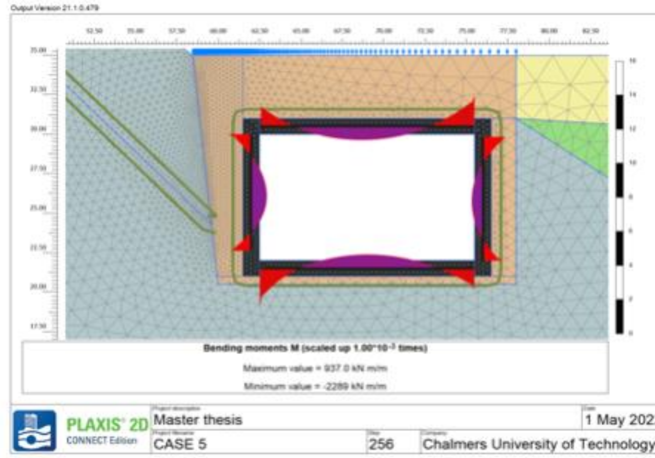
Bending moments M (scaled up 1.00*10^-3 times)
Maximum value = 937.0 kN m/m
Minimum value = -2289 kN m/m
PLAXIS 2D
CONNECT Edition
Master thesis
1 May 2022
CASE 5
256
Chalmers University of Technology

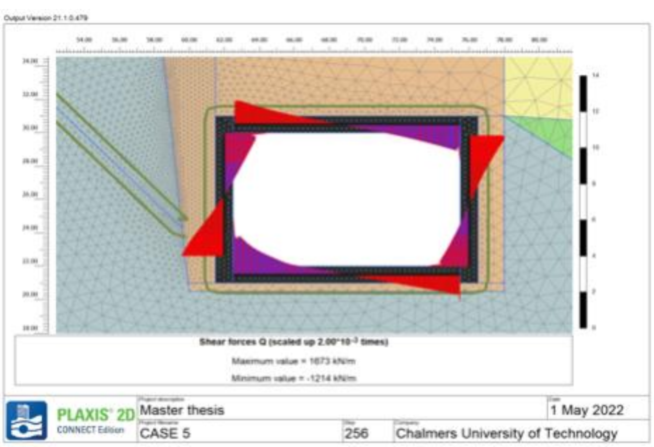
Shear forces Q (scaled up 2.00*10^-3 times)
Maximum value = 1673 kN/m
Minimum value = -1214 kN/m
PLAXIS 2D
CONNECT Edition
Master thesis
1 May 2022
CASE 5
256
Chalmers University of Technology

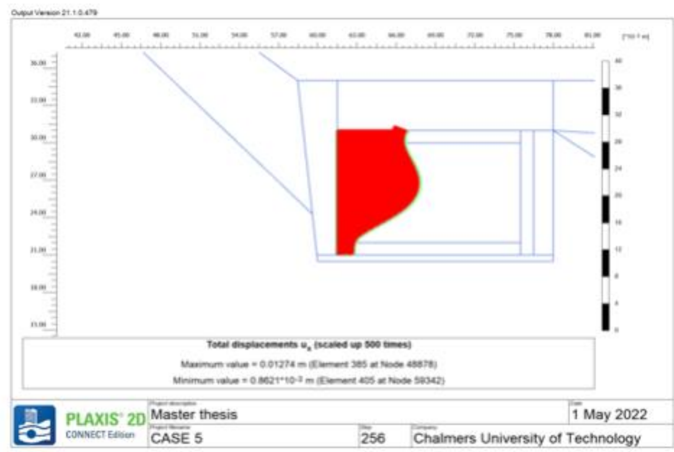
PLAXIS 2D
CONNECT Edition
Master thesis
1 May 2022
CASE 5
256
Chalmers University of Technology

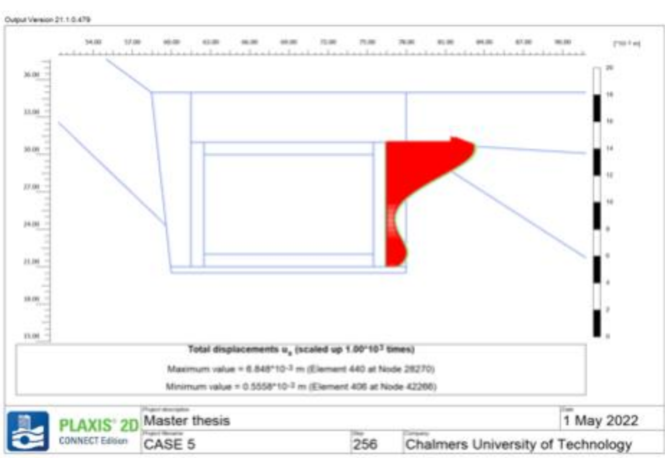
PLAXIS 2D
CONNECT Edition
Master thesis
1 May 2022
CASE 5
256
Chalmers University of Technology

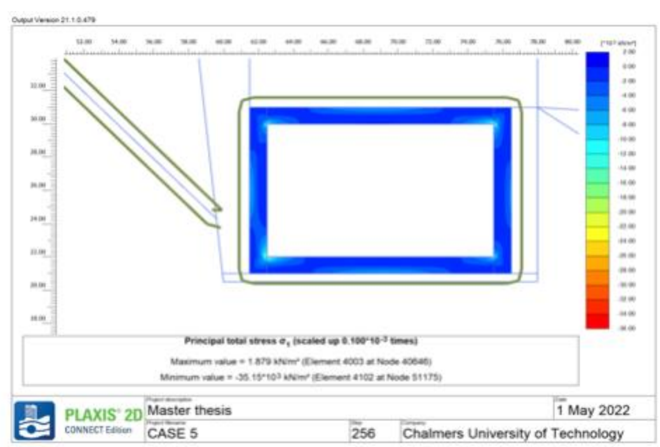
PLAXIS 2D
CONNECT Edition
Master thesis
1 May 2022
CASE 5
256
Chalmers University of Technology

2.5 Case 6

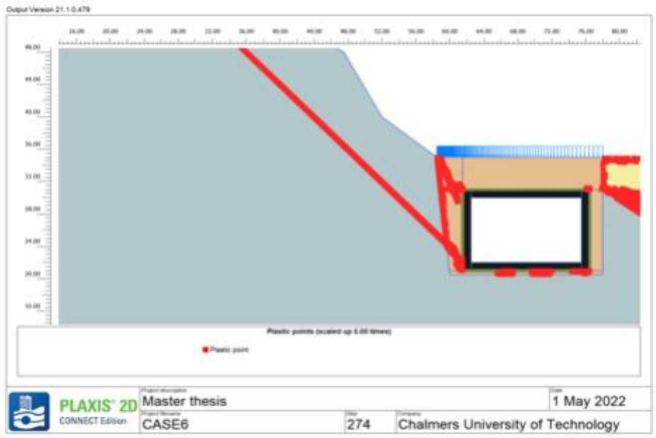
Plastic point
PLAXIS 2D
CONNECT Edition
Master thesis
1 May 2022
CASE6
274
Chalmers University of Technology

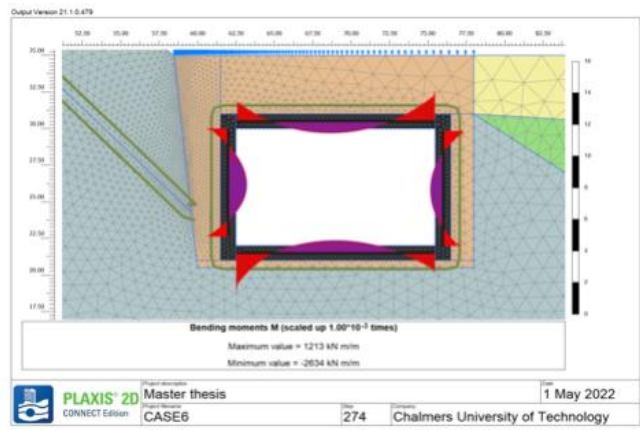
Bending moments M (scaled up 1.00*10^-3 times)
Maximum value = 1213 kN m/m
Minimum value = -2634 kN m/m
PLAXIS 2D
CONNECT Edition
Master thesis
1 May 2022
CASE6
274
Chalmers University of Technology

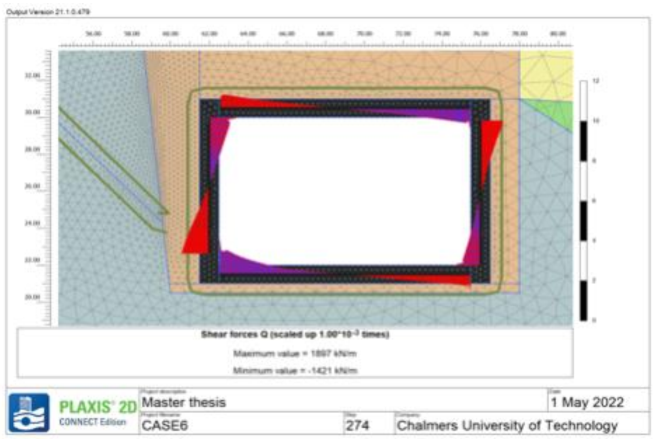
Shear forces Q (scaled up 1.00*10^-3 times)
Maximum value = 1897 kN/m
Minimum value = -1421 kN/m
PLAXIS 2D
CONNECT Edition
Master thesis
1 May 2022
CASE6
274
Chalmers University of Technology

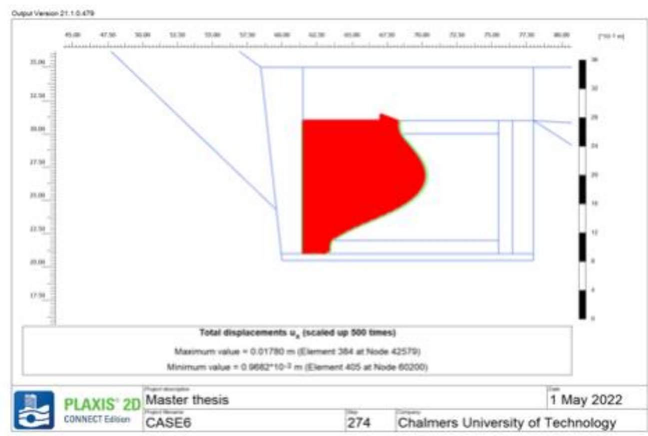
Total displacements u_x (scaled up 500 times)
PLAXIS 2D
CONNECT Edition
Master thesis
1 May 2022
CASE6
274
Chalmers University of Technology

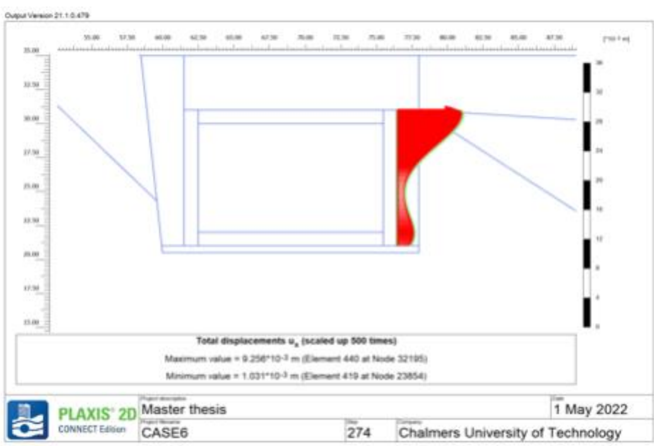
Total displacements u_x (scaled up 500 times)
PLAXIS 2D
CONNECT Edition
Master thesis
1 May 2022
CASE6
274
Chalmers University of Technology

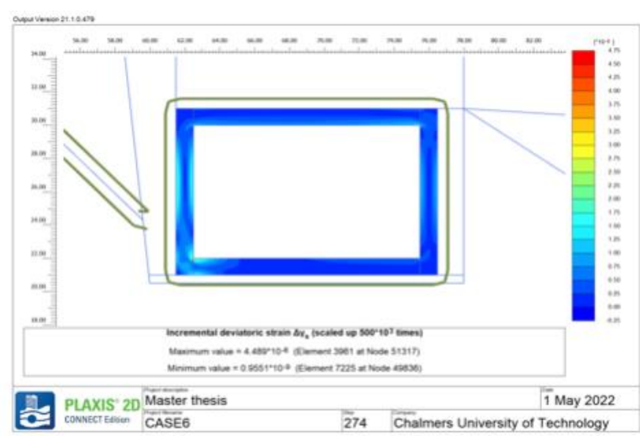
Incremental deviatoric strain
PLAXIS 2D
CONNECT Edition
Master thesis
1 May 2022
CASE6
274
Chalmers University of Technology

2.6 Case 7

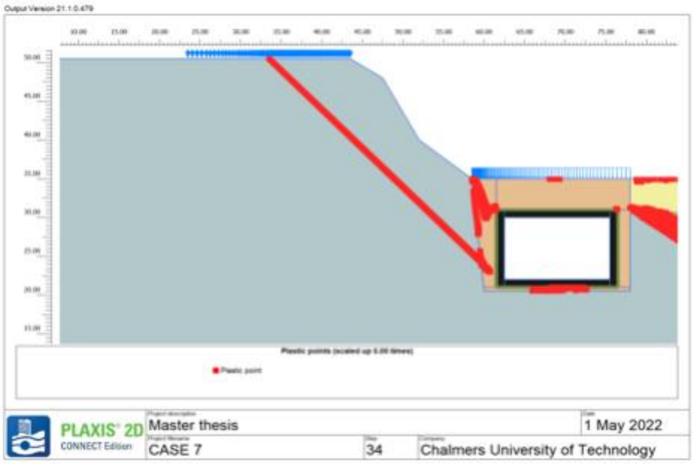
PLAXIS 2D
CONNECT Edition
Master thesis
1 May 2022
CASE 7
34
Chalmers University of Technology

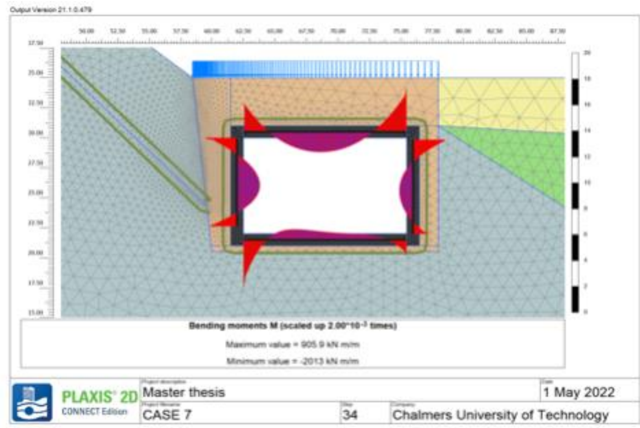
PLAXIS 2D
CONNECT Edition
Master thesis
1 May 2022
CASE 7
34
Chalmers University of Technology

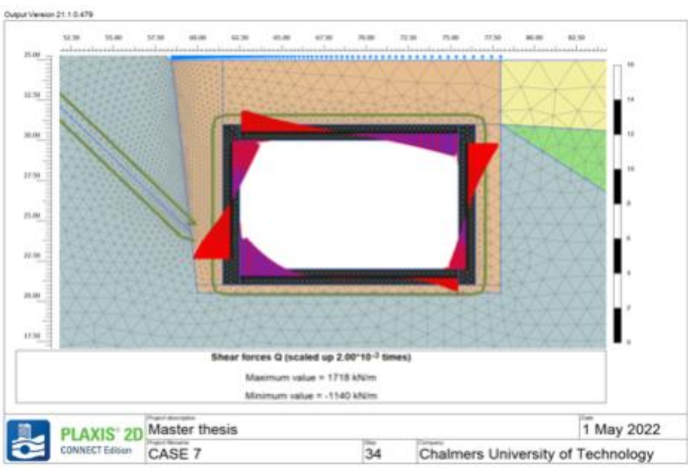
PLAXIS 2D
CONNECT Edition
Master thesis
1 May 2022
CASE 7
34
Chalmers University of Technology

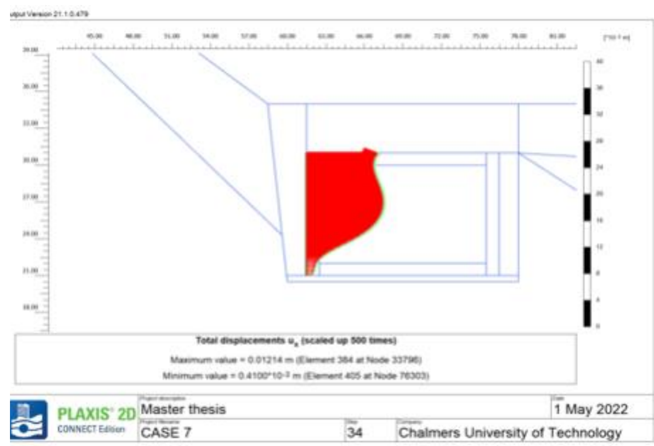
PLAXIS 2D
CONNECT Edition
Master thesis
1 May 2022
CASE 7
34
Chalmers University of Technology

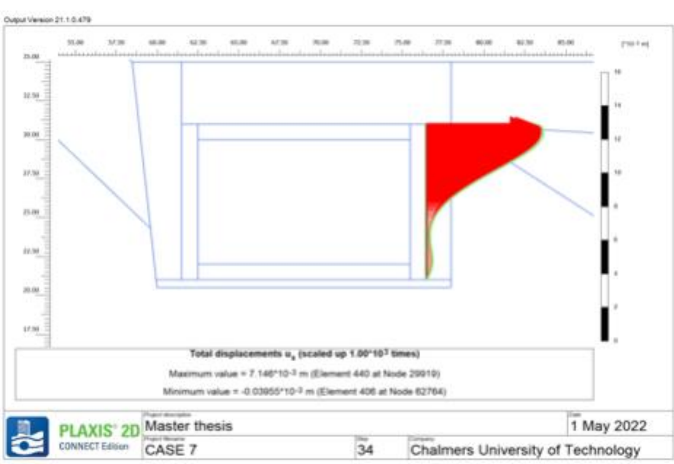
PLAXIS 2D
CONNECT Edition
Master thesis
1 May 2022
CASE 7
34
Chalmers University of Technology

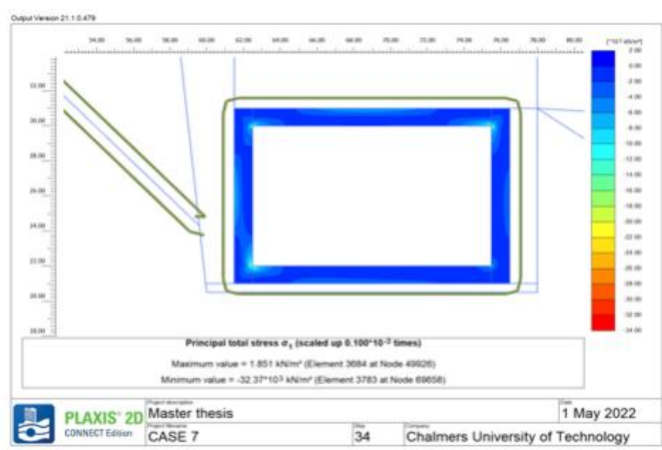
PLAXIS 2D
CONNECT Edition
Master thesis
1 May 2022
CASE 7
34
Chalmers University of Technology